Article

Cell Reports

Thrombopoietin Metabolically Primes Hematopoietic Stem Cells to Megakaryocyte-Lineage Differentiation

Graphical Abstract

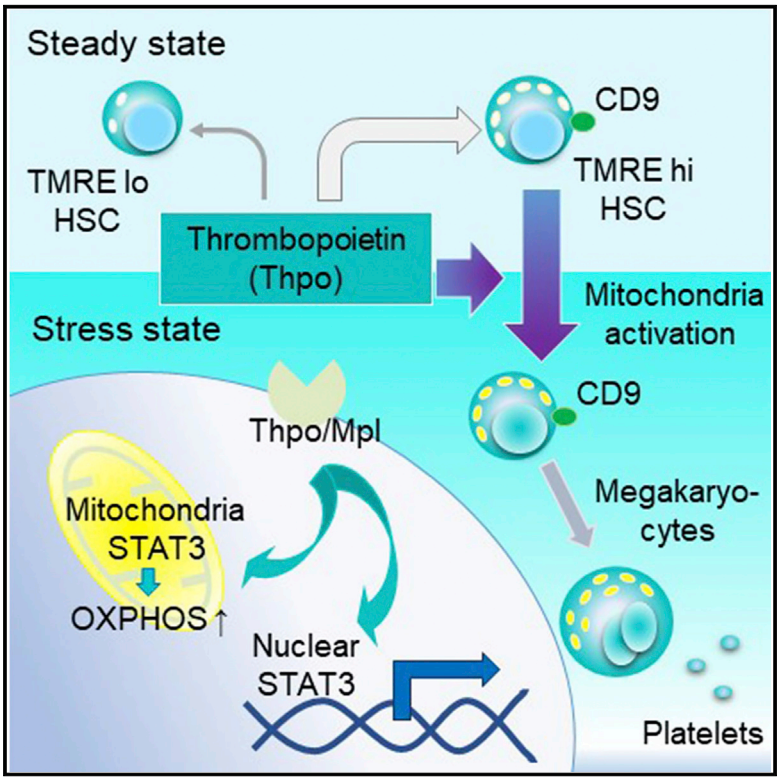

Highlights

- Thpo facilitates Mk-lineage differentiation through mitochondrial activation in HSCs
- Mitochondria-rich HSCs exhibit Mk-lineage differentiation
- Mitochondria-associated pSTAT3 is involved in mitochondria activation via Thpo signaling

Authors

Ayako Nakamura-Ishizu, Takayoshi Matsumura, Patrick S. Stumpf, ..., A'Qilah Banu Bte Abdul Majeed, Ben D. MacArthur, Toshio Suda

Correspondence

ayaknakm@gmail.com (A.N.-I.), sudato@keio.jp (T.S.)

In Brief

Nakamura-Ishizu et al. show that Thpo rapidly upregulates HSC mitochondrial activity in HSCs, an activity accompanied by preferential differentiation to an Mk lineage. Thpo-induced mitochondrial activity correlates with the tetraspanin CD9 expression pattern on HSCs. The findings suggest that Thpo-dependent changes in mitochondrial metabolism prime HSCs to undergo direct differentiation to an Mk lineage.

Nakamura-Ishizu et al., 2018, Cell Reports *25*, 1772–1785
November 13, 2018
https://doi.org/10.1016/j.celrep.2018.10.059

CellPress

OPEN ACCESS
CellPress

Cell Reports
Article

Thrombopoietin Metabolically Primes Hematopoietic Stem Cells to Megakaryocyte-Lineage Differentiation

Ayako Nakamura-Ishizu,[1,2,*] Takayoshi Matsumura,[1] Patrick S. Stumpf,[4] Terumasa Umemoto,[2] Hitoshi Takizawa,[2] Yuji Takihara,[1] Aled O'Neil,[1] A'Qilah Banu Bte Abdul Majeed,[1] Ben D. MacArthur,[2,3,4] and Toshio Suda[1,2,5,*]
[1]Cancer Science Institute, National University of Singapore, 14 Medical Drive, MD6, 117599 Singapore, Singapore
[2]International Research Center for Medical Sciences, Kumamoto University, 2-2-1 Honjo, Chuo-ku, Kumamoto City 860-0811, Japan
[3]Mathematical Sciences, University of Southampton, Southampton SO17 1BJ, UK
[4]Centre for Human Development Stem Cells and Regeneration, Faculty of Medicine, University of Southampton, Southampton SO17 1BJ, UK
[5]Lead Contact
*Correspondence: ayaknakm@gmail.com (A.N.-I.), sudato@keio.jp (T.S.)
https://doi.org/10.1016/j.celrep.2018.10.059

SUMMARY

During acute myelosuppression or thrombocytopenia, bone marrow (BM) hematopoietic cells respond rapidly to replenish peripheral blood platelets. While the cytokine thrombopoietin (Thpo) both regulates platelet production and maintains HSC potential, whether Thpo controls megakaryocyte (Mk)-lineage differentiation of HSCs is unclear. Here, we show that Thpo rapidly upregulates mitochondrial activity in HSCs, an activity accompanied by differentiation to an Mk lineage. Moreover, in unperturbed hematopoiesis, HSCs with high mitochondrial activity exhibit Mk-lineage differentiation *in vitro* and myeloid lineage-biased reconstitution *in vivo*. Furthermore, Thpo skewed HSCs to express the tetraspanin CD9, a pattern correlated with mitochondrial activity. Mitochondria-active HSCs are resistant to apoptosis and oxidative stress upon Thpo stimulation. Thpo-regulated mitochondrial activity associated with mitochondrial translocation of STAT3 phosphorylated at serine 727. Overall, we report an important role for Thpo in regulating rapid Mk-lineage commitment. Thpo-dependent changes in mitochondrial metabolism prime HSCs to undergo direct differentiation to an Mk lineage.

INTRODUCTION

In stress conditions, the blood system requires a rapid and pliant response by hematopoietic stem cells (HSCs) to restore homeostasis. Efficient and rapid production of megakaryocytes (Mks) and platelets is an essential response during stress hematopoiesis, as defective hemostasis is life-threatening. To meet this demand, bone marrow (BM) HSCs may commit directly or preferentially to the Mk-lineage (Woolthuis and Park, 2016). Recent studies revealing heterogeneity in HSC differentiation patterns have identified cells directly committed to the Mk-lineage within phenotypic HSC populations (Yamamoto et al., 2013; Notta et al., 2016). Moreover, the use of combinations of cell markers, including CD41, cKit, CD105, and von Willebrand factor (vWF), have identified multilineage repopulating HSCs with Mk-lineage-biased differentiation (Gekas and Graf, 2013; Shin et al., 2014; Grinenko et al., 2014; Pronk et al., 2007; Sanjuan-Pla et al., 2013). Nonetheless, mechanisms underlying direct HSC differentiation to the Mk-lineage remain unknown.

HSCs reside in a hypoxic niche and rely on anaerobic glycolysis for maintenance (Spencer et al., 2014; Simsek et al., 2010). Evidence suggests that mitochondrial metabolism is therefore suppressed in quiescent HSCs, as increased mitochondrial activity parallels the loss of HSC potential (Simsek et al., 2010; Mantel et al., 2010; Piccoli et al., 2005). Mitochondrial activity may also be correlated with HSC differentiation to specific hematopoietic lineages. For example, *Atg7* knockout mice exhibit decreased stem cell potential and abnormal myeloid proliferation due to decreased clearance and subsequent overload of mitochondria in the cytoplasm (Mortensen et al., 2011). Deletion of mitofusin, which results in defective mitochondrial fusion and tethering of mitochondria to the endoplasmic reticulum, blocks HSC lymphoid differentiation (Luchsinger et al., 2016). However, it is not known whether or how changes in mitochondrial activity affect Mk-lineage differentiation of HSCs, an activity that requires relatively high energy production for endomitosis and platelet production (Chen et al., 2013).

Thrombopoietin (Thpo) signaling in HSCs has a double-edged effect. During steady-state hematopoiesis, Thpo signaling maintains HSCs in a quiescent state (Yoshihara et al., 2007; Qian et al., 2007). However, Thpo is also considered an acute phase protein rapidly upregulated in inflammation and various stress hematopoietic conditions (Ceresa et al., 2007; Cerutti et al., 1999). Among cytokines, signaling by Thpo is the most potent stimulator of HSC entry into the cell-cycle entry, resulting in self-renewal divisions (Walter et al., 2015; Kovtonyuk et al., 2016). Thpo is also a major stimulator of megakaryopoiesis (Kaushansky, 2016). Thpo reportedly stimulates Mk-biased vWF^{+} HSCs to rapidly proliferate, indicating that Thpo is a key regulator of rapid Mk production from Mk-biased HSCs (Sanjuan-Pla et al., 2013). However, mechanisms underlying this activity have not been investigated.

Here, we report that *in vivo* Thpo administration to mice rapidly differentiated BM HSCs to Mks and upregulated HSC

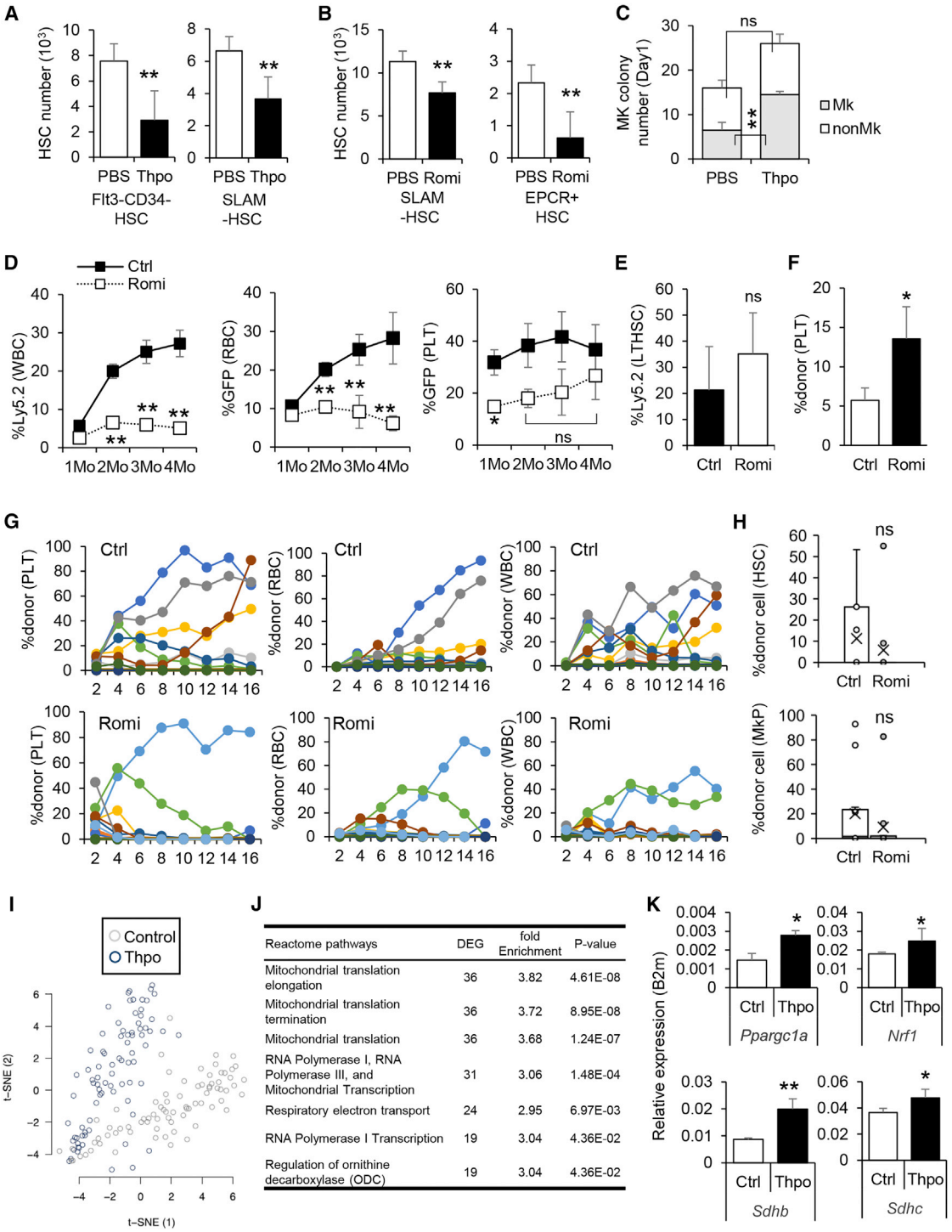

Reactome pathways	DEG	fold Enrichment	P-value
Mitochondrial translation elongation	36	3.82	4.61E-08
Mitochondrial translation termination	36	3.72	8.95E-08
Mitochondrial translation	36	3.68	1.24E-07
RNA Polymerase I, RNA Polymerase III, and Mitochondrial Transcription	31	3.06	1.48E-04
Respiratory electron transport	24	2.95	6.97E-03
RNA Polymerase I Transcription	19	3.04	4.36E-02
Regulation of ornithine decarboxylase (ODC)	19	3.04	4.36E-02

Figure 1. Thpo Signaling Rapidly Upregulates Mk Differentiation

(A) Relative cell number of SLAM ($CD150^+CD48^-$ LSK) HSCs and $Flt3^-CD34^-$ HSCs obtained from mice treated with PBS (control) or recombinant Thpo at day 1. Means ± SDs; n = 4; **p < 0.01 by Student's t test.

(B) Relative cell number of SLAM HSCs and endothelial protein C receptor-positive ($EPCR^+$) ($CD150^+CD48^-EPCR^+$ LSK) HSCs obtained from mice treated with PBS (control) or romiplostim (Romi) at day 1. Means ± SDs; n = 4; **p < 0.01 by Student's t test.

(C) Mk colony assay of 750 HSCs obtained from control or Thpo-treated mice. Means ± SDs; n = 4; **p < 0.01 by Student's t test.

(D) Monthly PB chimerisms of competitive BM transplantation of 500 HSCs from mice treated with Romi or PBS (Ctrl) for 1 day. HSCs were obtained from UBC-GFP mice (Ly5.2) and transplanted to Ly5.1 recipients with Ly5.1 competitor cells (mean ± SEM) (n = 5); *p < 0.05; **p < 0.01, ns, not significant by Student's t test.

(legend continued on next page)

mitochondrial function. HSCs with high mitochondrial activity exhibited preferential differentiation to Mk-lineage *in vitro*. Transplantation of BM harboring a small number of HSCs with high mitochondrial activity resulted in myeloid lineage-biased reconstitution. HSCs showing high mitochondrial activity were resistant to apoptosis and oxidative stress, predisposing them to rapid Mk differentiation upon Thpo stimulation. Our findings suggest that Thpo-induced mitochondrial activity primes HSCs to exit dormancy and directly differentiate along the Mk-lineage. These findings provide insight into the potential manipulation of HSCs *ex vivo* and could be particularly relevant to the production of Mk and platelets for blood transfusion.

RESULTS

Thpo Signaling Rapidly Upregulates Mk Differentiation

Cytokines are key players in recovery from hematopoietic stress. Among them, systemic Thpo levels fluctuate during acute stress hematopoiesis conditions, accompanied by thrombocytopenia. To assess changes in HSCs upon Thpo stimulation, we administered recombinant Thpo intravenously to adult wild-type (WT) mice and 1 day later analyzed cell populations by flow cytometry. In agreement with previous reports (Kabaya et al., 1996), Thpo administration promoted an increase in the number of peripheral blood (PB) platelets and Mk cells, which became apparent at day 5 of administration (Figures S1A–S1C). Although a single dose of Thpo did not alter PB platelet and BM Mk numbers (Figures S1A–S1C), the number of BM HSCs ($CD150^+CD48^-$ LSK [lineage negative, $Sca1^+$, $c\text{-}kit^+$] and CD34-Flt3-LSK) decreased after a single dose of Thpo administration (Figure 1A). Mice treated *in vivo* with romiplostim, a Thpo receptor (cMpl) agonist, showed similar changes in HSC number (Figures 1B and S1D). However, the number of cells in progenitor cell fractions, including Mk-lineage-committed Pre-MegE ($CD150^+CD105^-FcgRII/III^-CD41^-LKS^-$) and Mk-progenitor (MkP) ($CD41^+CD150^+LKS^-$), remained unchanged on day 1 after Thpo stimulation (Figure S1E). The decreased BM HSC number following a single dose of Thpo was not due to HSC mobilization from the BM (Figure S1F).

PB platelets are rapidly replenished during stress hematopoiesis (Li and Slayton, 2013). We therefore asked whether a single dose of Thpo promoted HSC differentiation toward an Mk-lineage. To do so, we assessed *in vitro* colony formation and found that BM HSCs obtained from Thpo-treated mice showed increased Mk colony output relative to HSCs from untreated mice (Figure 1C). A comparable analysis of mice treated with a single romiplostim dose also indicated increased Mk colony output (Figure S1G).

To assess lineage output *in vivo*, we derived HSCs from romiplostim-treated or -untreated ubiquitin (UBC)-GFP transgenic mice and competitively transplanted them into lethally irradiated Ly5.1 mice (Figure S1H). Donor HSCs from these mice harbor a GFP tag, enabling the evaluation of all hematopoietic lineages in recipients (Schaefer et al., 2001; Oguro et al., 2013). We first transplanted 500 HSCs from treated or untreated mice plus 4×10^5 competitor cells. Recipient mice transplanted with romiplostim-treated HSCs exhibited repopulation skewed toward platelet-lineage differentiation with a significant decrease in white blood cell (WBC) and red blood cell (RBC) reconstitution (Figure 1D). However, BM chimerism of HSCs at 4 months post-transplantation was comparable in romiplostim-treated and -untreated groups (Figure 1E). HSCs sorted by flow cytometry are heterogeneous and differ in repopulation and differentiation potential (Carrelha et al., 2018; Forsberg et al., 2005; Crisan and Dzierzak, 2016). Thus, we transplanted 20 HSCs from treated or untreated mice plus 2×10^5 competitor cells. Two weeks later, romiplostim-treated HSCs exhibited a high output of PB platelets relative to controls (Figures 1F and 1G). In terms of long-term reconstitution, romiplostim treatment generally reduced HSC reconstitution in WBCs, RBCs, and platelets (Figures 1G, S1I, and S1J); only one recipient in the romiplostim-treated group more than five recipients in the control group exhibited long-term multilineage repopulation. Overall, however, BM chimerism of HSCs, MkPs, and other progenitors at 4 months post-transplantation was comparable in romiplostim-treated and -untreated groups, although the former tended to repopulate recipient BM less efficiently than did control HSCs (Figures 1H and S1K). These data indicate that Thpo signaling rapidly reduces HSC potential and may promote differentiation to an Mk-lineage.

Thpo-Treated $CD41^+$ HSCs Show an Enhanced Mitochondrial Gene Signature

As Thpo injection rapidly alters the Mk-lineage output of HSCs, we asked whether Thpo signaling modulated genetic signatures seen in HSCs. Platelet integrin CD41 (αIIb) marks HSCs with myeloid-biased lineage differentiation potential (Gekas and Graf, 2013). Thus, we performed RNA sequencing of 96 single $CD41^+$ HSCs from control or Thpo-treated WT mice after 1 day and observed differential expression of 692 genes between groups (Figure S2A). Dimensionality reduction analysis using t-distributed stochastic neighbor embedding (t-SNE) (van der Maaten and Hinton, 2008) revealed no distinct clusters of cells within treatment groups but rather a broad shift in gene expression following Thpo stimulation (Figure 1I). Furthermore, $CD41^+$HSCs from Thpo-treated mice did not

(E) BM HSC chimerism in recipient mice. Means ± SDs; n = 5; ns, not significant by Student's t test.
(F–H) Competitive BM transplantation of 20 HSCs from mice treated with Romi or PBS (Ctrl) for 1 day. HSCs were obtained from UBC-GFP mice (Ly5.2) and transplanted to Ly5.1 recipients with Ly5.1 competitor cells. (F) Percentage of donor-derived platelets at 2 months after BM transplantation. Means ± SEMs; n > 10; *p < 0.05 by Student's t test. (G) Monthly PB chimerisms; n > 10. (H) BM HSC and MkP chimerism in recipient mice. Means ± SDs; n > 10; ns, not significant by Student's t test.
(I) t-SNE analysis on $CD41^+$ HSCs obtained from control and Thpo-treated mice.
(J) Overrepresentation of Reactome pathways gene sets among the differentially expressed genes between Thpo-treated and -untreated $CD41^+$ HSCs.
(K) Relative expression of mitochondria-related genes to *B2m* expression in HSCs sorted from PBS- (Ctrl) or Thpo-treated mice. Means ± SDs; n = 4; *p < 0.05, **p < 0.01 by Student's t test.

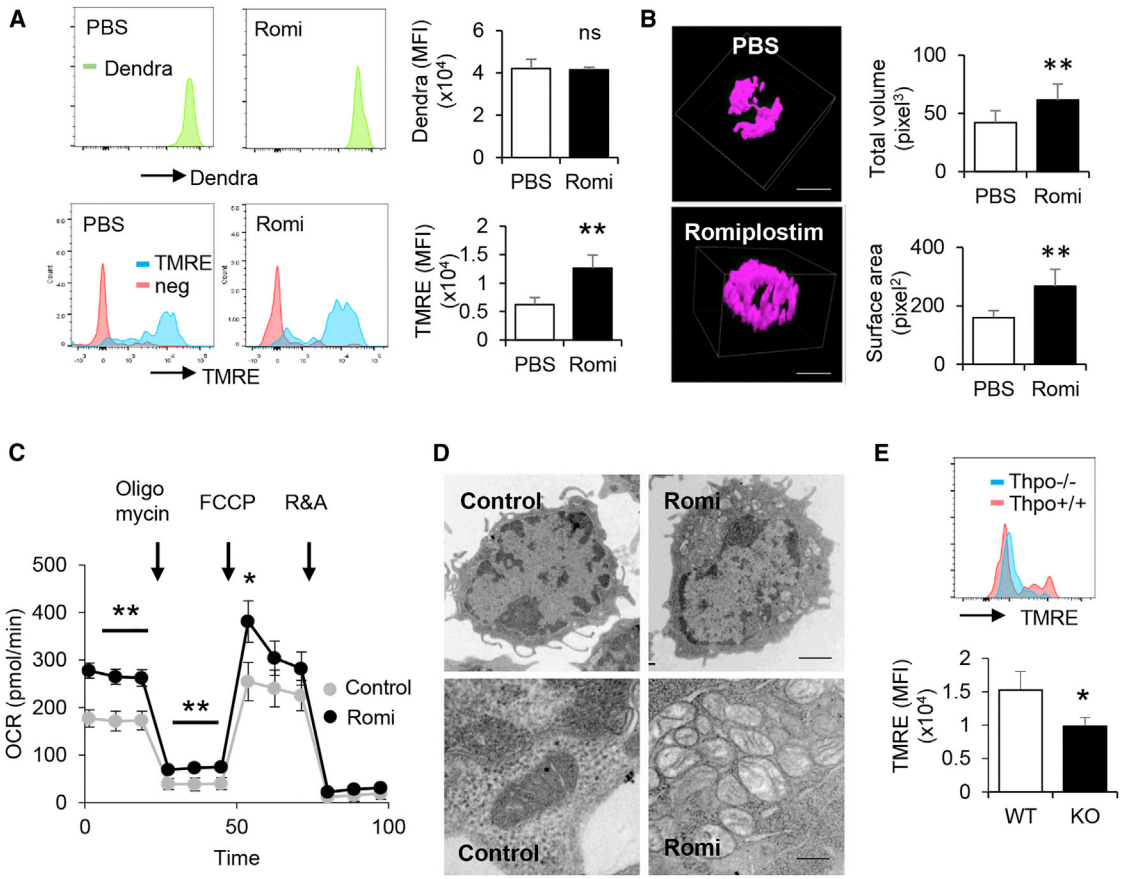

Figure 2. Thpo Induces Mitochondrial Activity in HSCs

(A) Representative flow cytometry plots and mean fluorescence intensity (MFI) of Dendra2 fluorescence and TMRE staining on HSCs obtained from treated with PBS (control) or romiplostim (Romi). Means ± SDs; n = 4; **p < 0.01, ns, not significant by Student's t test.

(B) Confocal images of single HSCs obtained from MitoDendra2 mice treated with PBS (control) or romiplostim (Romi). Scale bar, 5 μm. Pink regions highlight Dendra2^{+} regions used for volume and surface area measurements. Total volume and surface area of Dendra2^{+} mitochondria were quantified. Means ± SDs; n > 10; **p < 0.01 by Student's t test.

(C) Oxygen consumption rate (OCR) of LSK cells obtained from mice treated with PBS (control) or romiplostim (Romi). Means ± SDs; n = 3; *p < 0.05, **p < 0.01 by Student's t test. Cells were subjected to stimulation with oligomycin, FCCP, and rotenone and antimycin A (R&A).

(D) Transmission electron microscopy images of HSCs sorted from mice treated with PBS (control) or romiplostim (Romi). Scale bar, 2 μm (upper) and 0.2 μm (lower). Note that Romi-treated HSCs have mitochondria with clearer cristae structure in enlarged images (lower).

(E) Representative flow cytometry plot and mean fluorescence intensity (MFI) of TMRE staining on HSCs obtained from Thpo$^{-/-}$ and Thpo$^{+/+}$ HSCs. Means ± SDs; n = 4; *p < 0.05 by Student's t test.

exhibit significant changes in the expression of MkP- or Mk/erythrocyte progenitor (MEP)-associated gene sets (Sanjuan-Pla et al., 2013) relative to control HSCs (p = 0.7 and 1, respectively, with Fisher's exact test) (Figures S2B and S2C). However, gene set enrichment analysis (GSEA) of Reactome pathways using PANTHER (Mi et al., 2017) and Gene Ontology terms using GSEA (Broad Institute) (Mootha et al., 2003; Subramanian et al., 2005) revealed significant overrepresentation of mitochondria-associated gene sets (Figures 1J and S2D). qPCR of romiplostim-treated HSCs revealed a significantly high expression of genes related to mitochondrial biosynthesis and function, among them *Ppargc1a*, *Nrf1*, *Sdfb*, and *Sdhc* (Figure 1K). These data show that Thpo signaling rapidly enhances a mitochondrial genetic signature, while functionally encouraging an Mk-lineage bias.

Thpo Induces Mitochondrial Activity in HSCs

To confirm whether enhanced Thpo signaling alters mitochondrial mass or activity in HSCs, we assessed those activities in WT mice administered romiplostim or PBS (control). Mitochondrial mass, assessed using MitoTracker green (MTG) staining (Thermo Fisher Scientific), significantly increased in HSCs 1 day after romiplostim administration (Figure S3A). Because MitoTracker dyes are subject to dye efflux (de Almeida et al., 2017), we also assessed these changes in Mito-Dendra2 transgenic (photo-activatable mitochondria [Pham]) mice. HSCs from Mito-Dendra2 mice did not show change in the Dendra2 fluorescence signal detected with flow cytometry after a single dose of romiplostim (Figure 2A). Romiplostim-treated HSCs did, however, show a significantly greater mitochondrial volume and surface area per cell when assessed not using fluorescence

signal intensity but by the calculation of total volume using confocal microscopy (Figure 2B).

We next evaluated mitochondrial activity in various assays in HSCs from romiplostim-treated mice. First, we assessed changes in mitochondrial membrane potential using tetramethylrhodamine ethyl ester (TMRE) staining of BM HSCs from mice treated with one dose of romiplostim. One day after drug treatment, HSCs showed upregulated TMRE staining relative to untreated controls (Figure 2A), indicating increased mitochondrial membrane potential. Moreover, 1 day after romiplostim treatment, HSCs from treated mice showed significant upregulation in reactive oxygen species (ROS) levels, based on CellROX staining (Figure S3B). Seahorse analysis (Agilent) of 330,000 hematopoietic stem and progenitor cells (HSPCs) from romiplostim-treated versus control mice confirmed increased mitochondrial metabolism (oxygen consumption rate [OCR]) (Figure 2C). In addition, analysis of mitochondrial ultrastructure by transmission electron microscopy indicated that mitochondria in HSCs from romiplostim-treated mice exhibited more clear cristae structure compared to the mitochondria of untreated HSCs (Figure 2D). In agreement, HSCs derived from adult Thpo$^{-/-}$ mice exhibited significantly decreased TMRE staining relative to HSCs from Thpo$^{+/+}$ (Figure 2E). To determine whether signaling by other cytokines alters mitochondrial activity, we cultured HSCs from WT mice for 2 days with stem cell factor (SCF) or Thpo. HSCs cultured with Thpo showed significantly upregulated TMRE staining compared to HSCs cultured with SCF (Figure S3C). Furthermore, HSCs obtained from mice treated 5 days with granulocyte-colony-stimulating factor (G-CSF) showed mitochondrial mass comparable to that from untreated mice (Figure S3D). Overall, these data indicate that Thpo is a specific and potent stimulator of HSC mitochondrial synthesis and activity.

HSCs with High Mitochondrial Activity Exhibit a Myeloid-Lineage Bias

Steady-state HSCs are quiescent and remain in a low metabolic state (Nakamura-Ishizu et al., 2014). However, when we assessed steady-state HSCs for mitochondrial activity, we observed populations of cells with high and low mitochondria function (Figure S4A). Purified TMRE^{hi} HSCs exhibited lower electron density and more clear cristae structure compared to TMRE^{lo} HSCs under transmission electron microscope imaging (Figure 3A). Given that Thpo stimulates Mk-lineage differentiation and mitochondrial function, we asked whether mitochondrial activity in steady-state HSCs was correlated with Mk-lineage-biased hematopoiesis. To do so, we cultured TMRE^{hi} or TMRE^{lo} HSCs from WT mice for 4 days and assessed Mk differentiation using CD41 staining. Large CD41^{+} Mks were seen in the TMRE^{hi} HSC population but were not apparent in TMRE^{lo} HSC cultures (Figures 3B and S4B). Colony-forming assays also revealed higher numbers of Mk colonies from TMRE^{hi} HSCs compared to TMRE^{lo} HSCs (Figure 3C). To compare *in vivo* reconstitution potential between groups, we competitively transplanted 20 TMRE^{hi} or TMRE^{lo} HSCs purified from UBC-GFP mice into lethally irradiated Ly5.1 recipients. TMRE^{lo} HSCs reconstituted highly for all three blood lineages, yet TMRE^{hi} HSCs exhibited generally high reconstitution of platelets and RBC compared to WBC (Figures 3D, S4C, and S4D). Among WBC lineages, TMRE^{hi} HSCs exhibited higher repopulation in myeloid lineages than in lymphoid lineages (Figures S4E and S4F). TMRE^{hi} HSCs exhibited low but statistically not significant reconstitution of BM HSCs (Figure 3E). While reconstitution of BM MkP cells, along with GMP and erythroid progenitors, did not differ between TMRE^{hi} and TMRE^{lo} HSCs, TMRE^{hi} HSCs exhibited a significantly low repopulation of common lymphoid progenitor (CLP) cells compared to TMRE^{lo} HSCs (Figures 3E and S4G). These data indicate that high mitochondrial activity may prime HSCs toward myeloid-biased reconstitution and rapid Mk-lineage differentiation.

Thpo Signaling Upregulates CD9 Expression in HSCs

Single-cell RNA sequence analysis (Figure 1) did not reveal distinct clustering of HSC populations within myeloid-biased CD41^{+} HSCs. Therefore, to further characterize Thpo-stimulated HSCs and better subfraction these cells, we used single-cell mass cytometry (CyTOF) for the expression of various HSC-, Mk- and metabolism-related markers in BM cells obtained from control or romiplostim-treated mice. t-Distributed stochastic linear embedding (t-SNE) analysis of LSK cells from romiplostim-treated mice indicated a shift in expression of 27 markers (Figures 4A and S5A). Relevant to individual markers, the expression of HSC markers (Tie2, CD150, EPCR, CD105, and Mpl) was concentrated in two clusters (Figure 4A). One dose of romiplostim significantly decreased the number of cells in the cluster marked with a blue line, but the cells in the cluster marked with a red line remained unchanged (Figure 4A). Expression of Mk-lineage markers (CD41, CD9, and CD61) was concentrated in the bottom cluster, along with expression of several factors functioning in metabolism-related pathways (phospho-5′ AMP-activated protein kinase [pAMPK], pMAPKAPK2, and phosphoAKT [pAKT]). To further assess the effect of romiplostim administration on the expression of individual proteins, a simple machine-learning classifier known as Random Forest was trained to distinguish between HSCs from the two treatment groups. This classifier was able to predict whether a cell had been exposed to romiplostim with high certainty (area under the curve [AUC] = 0.92; see Figure S5B) and ranked features based on their discriminative power using the mean decrease in the Gini index. This analysis confirmed that the protein expression of multiple Mk-associated markers (CD9, CD41, cMpl, and CD61) were strong indicators of the early segregation of MK-primed HSCs following romiplostim treatment (Figure S5C). While the greatest change was in decreased cMpl expression, we observed a significant increase in CD9 expression in romiplostim-treated HSCs relative to control HSCs (CD150^{+}CD48^{-}LSK cells) (Figure 4B). We confirmed upregulated CD9 expression on HSCs treated with either romiplostim or recombinant Thpo by flow cytometry (Figures 4C and S5D). These data indicate that Thpo signaling robustly alters protein expression in HSCs and skews them toward Mk-related phenotypes.

CD9^{hi} HSCs Are Mitochondria Rich and Differentiate into Mk Cells

Given that Thpo signaling enhances CD9 expression, we assessed a potential correlation between CD9 expression and

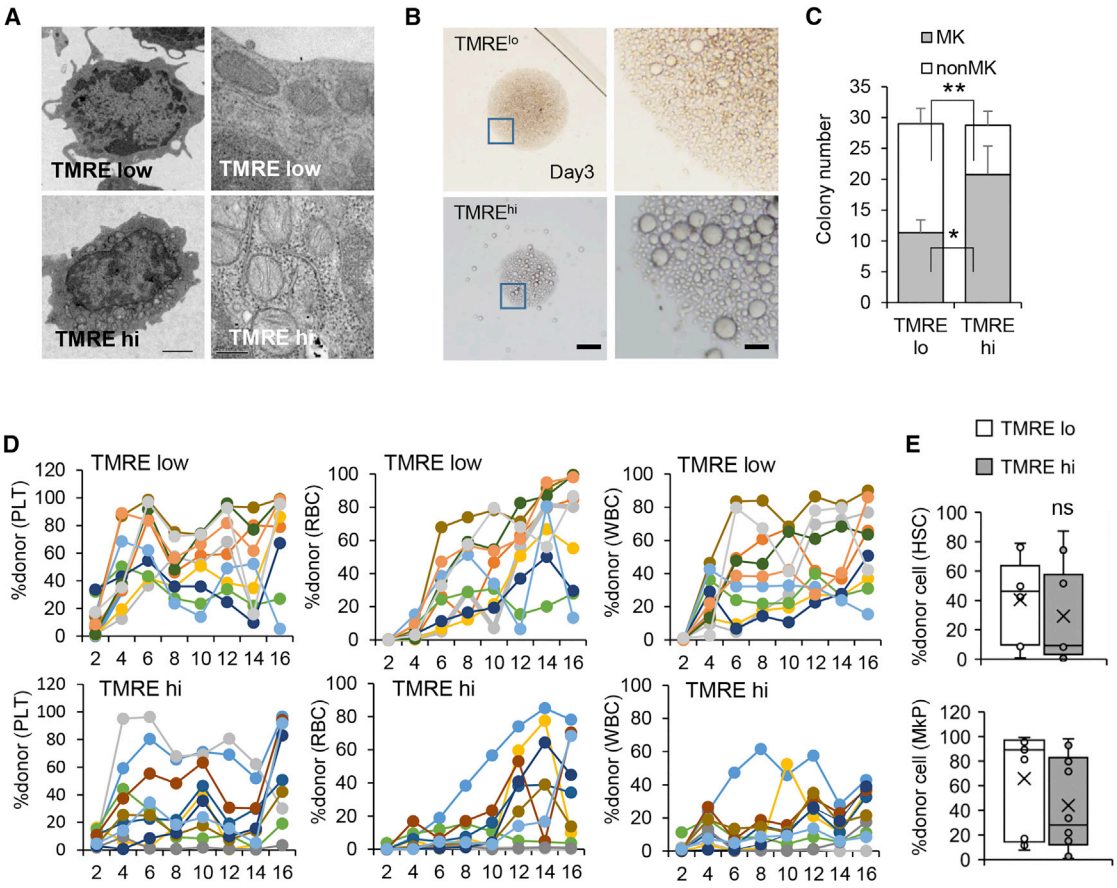

Figure 3. HSCs with High Mitochondrial Activity Differentiate to Mks

(A) Transmission electron microscopy images of TMRE^{hi} or TMRE^{lo} HSCs. Note that TMRE^{hi} HSCs have mitochondria with clear cristae structure in enlarged images (lower). Scale bar, 2 μm (left) and 0.2 μm (right).

(B) Culture images of 5000 TMRE^{lo} or TMRE^{hi} HSCs cultured for 3 days in Thpo-containing medium. Enlargement of blue square areas at right. Scale bar, 500 μm (left) and 50 μm (right).

(C) Mk colony assay of 750 TMRE^{hi} and TMRE^{lo} HSCs obtained from mice. Means ± SDs; n = 4; *p < 0.05, **p < 0.01 by Student's t test.

(D) Monthly PB chimerisms of competitive BM transplantation of 20 TMRE^{hi} or TMRE^{lo} HSCs. HSCs were obtained from UBC-GFP mice (Ly5.2) and transplanted to Ly5.1 recipients with Ly5.1 competitor cells. Means ± SDs; n > 10.

(E) BM HSC and MkP chimerism in recipient mice. Means ± SDs; n > 10; ns, not significant by Student's t test.

mitochondrial activity. Compared to CD9^{lo} HSCs, CD9^{hi} HSCs showed significantly high TMRE staining but comparable Dendra2 fluorescence (Figures 4D and S5E). CD9^{hi} HSCs were also significantly positive for MTG and CellROX staining (data not shown). Furthermore, we observed upregulation of mitochondrial biosynthesis and function-related genes (*Tfam*, *Atp5a*, *Cox5a*, and *Cyc1*) in CD9^{hi} relative to CD9^{lo} HSCs (Figure 4E). CD9^{hi} HSCs also exhibited relatively higher levels of intracellular ATP, which is indicative of increased mitochondrial activity (Figure S5F). Moreover, ultrastructural analysis revealed mitochondria in the cytoplasm of CD9^{hi} HSCs, the morphology of which resembled that of TMRE^{hi} or romiplostim-treated HSCs (Figure 4F).

We next characterized Mk-lineage differentiation of CD9^{hi} HSCs *in vitro* and found that CD9^{hi} HSCs formed a significantly greater percentage of Mk colonies than did CD9^{lo} HSCs (Figure S5G). CD9^{hi} HSCs also gave rise to a greater number of Mk cells than did CD9^{lo} HSCs when cultured with Thpo for 3 days (Figures S5H and S5I). These data indicate that CD9^{hi} HSCs correspond to a subgroup of Mito^{hi} HSCs enriched in Mk-lineage differentiation potential and are metabolically activated by Thpo.

High Mitochondrial Function Is Critical for Mk Differentiation

To assess how high mitochondrial activity in HSCs correlates with Mk differentiation, we inhibited mitochondrial synthesis by culturing HSCs for 3 days with or without carbonyl cyanide *p*-trifluoromethoxyphenylhydrazone (FCCP), which uncouples mitochondrial oxidative phosphorylation and ATP synthesis (Guimarães et al., 2012). FCCP treatment reduced HSC TMRE staining and ATP production (Figures 5A and 5B) and significantly decreased HSC and Mk frequency in the culture (Figures 5C and 5D). Functionally, FCCP-treated HSCs exhibited

significantly decreased Mk colony output (Figure 5E). We also inhibited AMPK, which stimulates mitochondrial biosynthesis in conditions of energy deprivation and cytokine stimulation (Burkewitz et al., 2014), by treating HSCs for 1 day with the AMPK inhibitor Compound C at 0.1 and 1 μM or vehicle (DMSO) (Mihaylova and Shaw, 2011; Stetler et al., 2012). Compound C treatment decreased MitoTracker staining as well as $CD9^{hi}$ HSC frequency within the culture (Figures S6A and S6B). Compound C-treated HSCs also produced fewer Mk colonies relative to DMSO-treated controls (Figure S6C). These data indicate that enhanced mitochondrial synthesis may drive HSCs toward Mk-lineage differentiation.

High Mitochondrial Function following Thpo Signaling Is Associated with HSC Proliferation and Survival

As Thpo induces HSC proliferation (Walter et al., 2015), we asked whether mitochondrial activity is related to HSC cell-cycle status. To avoid fixation-related problems with staining (Guimarães et al., 2012), we used Fucci transgenic mice, in which hematopoietic cells express Azami-Green (mAG) in S/G2/M phase (Tomura et al., 2013). One day after the administration of romiplostim to mice, we observed an increased frequency of mAG^{+} HSCs in BM (Figure 5F). When $TMRE^{hi}$ and $TMRE^{lo}$ HSCs were cultured for 1 day, $TMRE^{hi}$ HSCs exhibited significantly higher mAG frequency compared to $TMRE^{lo}$ HSCs (Figure 5G). Also, steady-state $CD9^{hi}$ and $CD9^{lo}$ HSCs showed a comparable frequency of cells in S/G2/M phase (Figure S6D), while upon Thpo stimulation, $CD9^{hi}$ HSCs exhibited significantly increased mAG positivity (Figure S6D). These data indicate that upon Thpo stimulation, mitochondria-active HSCs respond rapidly and exhibit greater proliferation than other HSC subpopulations.

Cytokine signaling can provoke apoptosis along with cell-cycle progression (Croker et al., 2015; Ruscetti and Bartelmez, 2001). We therefore asked whether Thpo-stimulated HSC cell-cycle progression was accompanied by apoptosis and whether mitochondrial activity regulated apoptotic activity. BM HSCs showed significantly increased annexin V staining and caspase-3 expression after 1 day of romiplostim administration, indicating that Thpo signaling induces apoptosis (Figure 5H). $TMRE^{hi}$ HSCs exhibited a significantly lower frequency of annexin V^{+} cells compared to $TMRE^{lo}$ HSCs (Figure 5I). The pro-apoptotic genes *Bax*, *Bak1*, and *Bcl2* were also downregulated in $TMRE^{hi}$ HSCs (Figure 5J). Mitochondrial activity induces oxidative stress, promoting apoptosis (Ott et al., 2007). $TMRE^{hi}$ HSCs cultured in Thpo for 3 days exhibited significantly higher levels of the antioxidant genes *Prdx1*, *Prdx3*, *Gpx1*, *Gpx4*, and *Txn2* compared to $TMRE^{lo}$ HSCs (Figure S6E), suggesting that $TMRE^{hi}$ HSCs are resistant to the oxidative stress associated with proliferation. These data indicate that mitochondria-active HSCs are highly proliferative but survive proliferative stress.

Mitochondria-Associated pSTAT3 Is Upregulated in Mitochondria-Active HSCs

Thpo signals by binding its receptor Mpl (Gurney et al., 1994). Therefore, we asked whether Mpl expression correlates with Thpo-induced mitochondrial function. We cultured Mpl^{hi} and Mpl^{lo} HSCs with or without Thpo for 3 days and found that Mpl^{hi} HSCs showed high TMRE staining when cultured without Thpo, but that the addition of Thpo to cultures increased TMRE staining in both Mpl^{hi} and Mpl^{lo} HSCs (Figure 6A). Mk colony output of Mpl^{hi} or Mpl^{lo} HSCs cultured with Thpo was comparable (Figure 6B). We conclude that both Mpl^{hi} and Mpl^{lo} HSCs respond equally to Thpo *in vitro*.

Finally, we asked what downstream signals mediate HSC mitochondrial function in response to Thpo. Selinexor (KPT-330) has been used recently to confine phospho-signal transducer and activator of transcription 3 (pSTAT3) to the HSC nucleus by inhibiting exportin 1 (XPO1)-mediated translocation to the cytoplasm and alter Mk differentiation (Machlus et al., 2017). HSCs purified from WT mice were cultured 3 days with or without KPT-330. KPT-330 treatment significantly inhibited mitochondrial activity based on TMRE staining and decreased HSC ATP production (Figures 6C and 6D). Treatment also significantly decreased the frequency of $CD41^{+}$ cells within the culture (Figure 6E), and HSCs cultured with KPT-330 exhibited significantly reduced Mk colony output (Figure 6F).

While acting primarily as nuclear transcription factors, STAT proteins reportedly exert extranuclear functions (Meier and Larner, 2014). STAT3 phosphorylated at serine 727 (S727) is transported to mitochondria and stimulates mitochondrial function by activating complexes I and II of the electron transport chain (Wegrzyn et al., 2009; Kramer et al., 2015). We therefore asked whether Mk-biased HSCs express higher levels of pSTAT3 (S727) using flow cytometry. pSTAT3 (S727) expression was significantly upregulated in HSCs obtained from romiplostim-treated mice relative to controls (Figure 6G), and pSTAT3 (S727) expression was comparable in $TMRE^{hi}$ and $TMRE^{lo}$ HSCs from WT mice (Figure 6H). However, when sorted $TMRE^{hi}$ or $TMRE^{lo}$ HSCs were cultured in the presence of Thpo, $TMRE^{hi}$ HSCs significantly upregulated pSTAT3 (S727) expression relative to $TMRE^{lo}$ HSCs (Figure 6I). We next used super-resolution imaging (stochastic optical reconstruction microscopy [STORM]) to define the subcellular localization of pSTAT3 (S727) in HSCs. Mitochondria-rich ($TMRE^{hi}$) HSCs treated with Thpo exhibited pSTAT (S727) signals in mitochondria, which were stained with the TOMM20 antibody (Figure 6J). The complex I subunit, gene associated with retinoid interferon (IFN)-induced cell mortality-19 (GRIM-19), recruits STAT3 to mitochondria (Tammineni et al., 2013). $TMRE^{hi}$ HSCs exhibited higher expression of GRIM-19 (Ndufa13) relative to $TMRE^{lo}$ HSCs (Figure 6K). Moreover, mitochondria-rich HSCs exhibited significantly higher expression of GRIM-19 protein (Figure 6L). These data suggest that upregulated mitochondrial function following Thpo stimulation may be associated with non-nuclear pSTAT3 signaling.

DISCUSSION

Here, we show that upon upregulation of Thpo signaling, HSCs rapidly upregulate mitochondrial activity, an activity accompanied by the induction of Mk-lineage differentiation. We observed that HSC mitochondrial activity is also correlated with myeloid-biased hematopoiesis and Mk-lineage output in steady-state HSCs. Mitochondria-rich HSCs rely on high energy production for Mk-lineage differentiation and cell proliferation. Mitochondria-rich HSCs resist apoptosis and oxidative stress upon

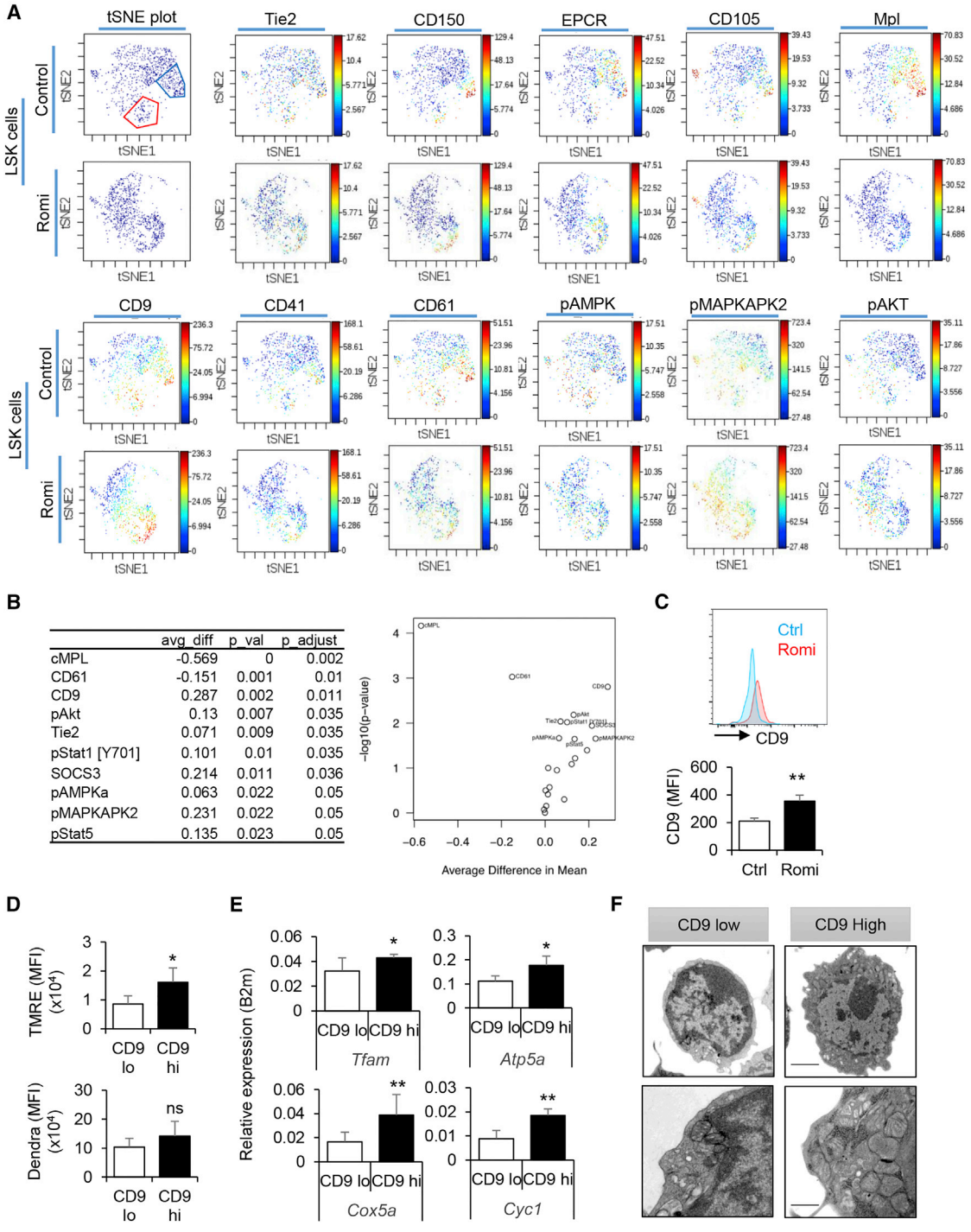

Figure 4. Thpo-Stimulated and Mitochondria-Abundant HSCs Express CD9

(A) Representative t-SNE plot showing the distribution of various HSCs, Mk surface markers, and downstream pathway molecules in LSK cell fractions obtained from mice treated with PBS (control) or romiplostim (Romi). Note that HSC populations (Tie2$^+$, CD150$^+$, EPCR$^+$, CD150$^+$, and Mpl$^+$) cells concentrate in two cellular clusters marked within red and blue lines; n = 4.

(B) Average difference in means and p values between control and Romi-treated HSCs (CD150$^+$CD48$^-$ LSK cells); n = 4.

(C) Representative flow cytometry plots and MFI for CD9 in HSCs obtained from mice treated with PBS (control) or romiplostim (Romi). Means ± SDs; n = 4; **p < 0.01 by Student's t test.

(legend continued on next page)

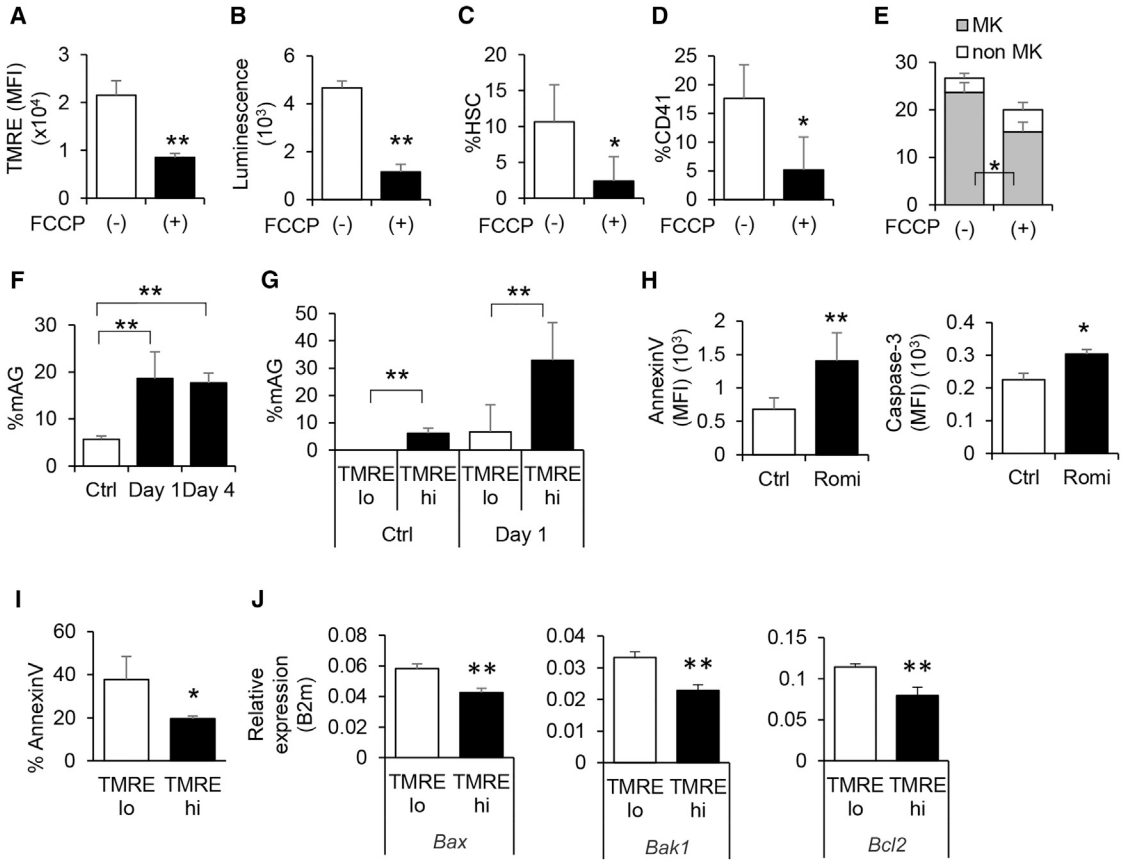

Figure 5. High Mitochondria Function Is Critical for HSC Survival and Mk Differentiation

(A) Mean fluorescence intensity (MFI) of TMRE staining on HSCs cultured with or without FCCP. Means ± SDs; n = 5; **p < 0.01 by Student's t test.

(B) Luminescence showing cellular ATP content in HSCs cultured with or without FCCP. Means ± SDs; n = 5; **p < 0.01 by Student's t test.

(C and D) Percentage of HSCs (C) and CD41^{+} cells (D) after 3-day culture of HSCs with or without FCCP. Means ± SDs; n = 5; *p < 0.05 by Student's t test.

(E) Mk colony assay of 750 HSCs obtained from FCCP (–) or (+) culture. Means ± SDs; n = 4; *p < 0.05 by Student's t test.

(F) Percentage of HSCs that are mAG^{+} in control or days 1 and 4 of romiplostim injection. Means ± SDs; n = 5; **p < 0.01 by Tukey's test.

(G) Percentage of TMRE^{hi} or TMRE^{lo} HSCs that are positive HSCs in control (Ctrl) or day 1 after romiplostim injection. Means ± SDs; n = 5; **p < 0.01 by Tukey's test.

(H) MFI of annexin V and cleaved caspase-3 expression in HSCs obtained from mice treated with PBS (Ctrl) or romiplostim (Romi) at day 1; n = 4; *p < 0.05, **p < 0.01 by Student's t test.

(I) Percentage of annexin V^{+} cells in TMRE^{hi} or TMRE^{lo} HSCs cultured in medium containing recombinant Thpo; n = 4; *p < 0.05 by Student's t test.

(J) Relative expression of apoptosis-related genes to B2m expression in TMRE^{hi} or TMRE^{lo} HSCs cultured in medium containing recombinant Thpo. Means ± SDs; n = 4; **p < 0.01 by Student's t test.

replicative stress induced by Thpo. Finally, we characterized signaling downstream of Thpo that may enhance mitochondrial function in HSCs.

HSCs reside in a hypoxic niche and rely on glycolysis for steady-state energy production (Spencer et al., 2014; Takubo et al., 2010). Nevertheless, past work has shown that steady-state HSCs have variable mitochondrial content (Simsek et al., 2010; Vannini et al., 2016). Furthermore, HSC function significantly declines in mice with defective mitochondrial respiration (Ansó et al., 2017; Liu et al., 2017), indicating that mitochondrial activity is essential for HSC maintenance. We also report that, in addition to repopulation potential, the heterogeneity of mitochondrial activity in HSCs also affects lineage output. We also observed that HSC mitochondrial biosynthesis and Mk-lineage bias was driven post-5-fluorouracil (5-FU) administration (data not shown), supporting the idea that this pathway is essential

(D) Mean fluorescence intensity (MFI) of Dendra2 fluorescence and TMRE staining on CD9^{lo} and CD9^{hi} HSCs obtained from treated with PBS (control) or romiplostim (Romi). Means ± SDs; n = 5; *p < 0.05; ns, not significant by Student's t test.

(E) Relative expression of mitochondria-related genes to *B2m* expression in CD9^{lo} and CD9^{hi} HSCs sorted from PBS- (Ctrl) or Thpo-treated mice. Means ± SDs; n = 4; *p < 0.05, **p < 0.01 by Student's t test.

(F) Transmission electron microscopy images of CD9^{lo} and CD9^{hi} HSCs. Scale bar, 2 μm (upper) and 0.2 μm (lower).

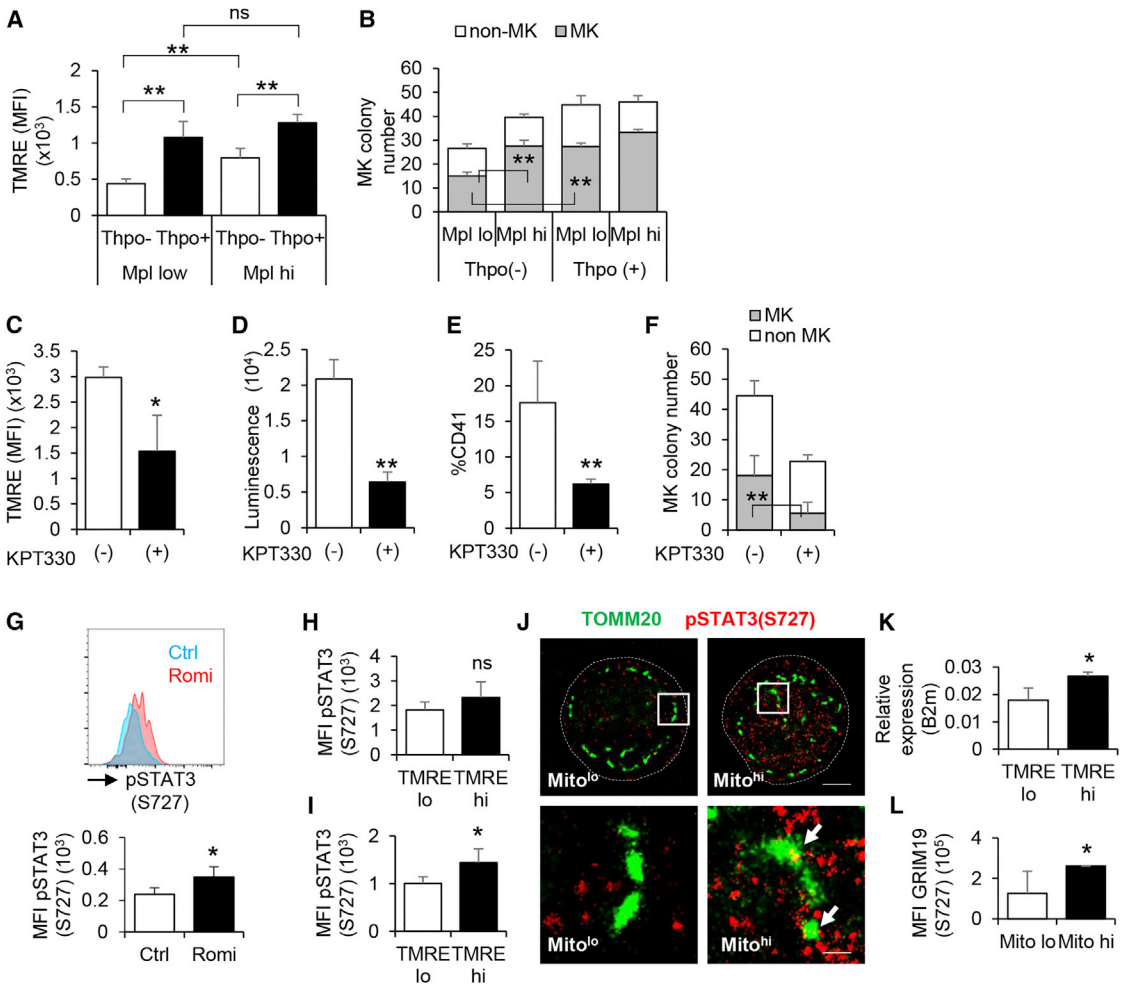

Figure 6. Mitochondria-Associated pSTAT3 Is Upregulated in Mk-Differentiating HSCs

(A) Mean fluorescence intensity (MFI) of TMRE staining on Mpl^{lo} and Mpl^{hi} HSCs cultured in medium with or without recombinant Thpo. Means ± SDs; n = 5; **p < 0.01, ns, not significant by Tukey's test.

(B) Mk colony assay of 750 HSCs obtained from Mpl^{lo} and Mpl^{hi} HSCs cultured in medium with or without recombinant Thpo. Means ± SDs; n = 4; **p < 0.01 by Student's t test.

(C) Mean fluorescence intensity (MFI) of TMRE staining on HSCs cultured with or without KPT-330. Means ± SDs; n = 5; *p < 0.05 by Student's t test.

(D) Luminescence showing cellular ATP content in HSCs cultured with or without KPT-330. Means ± SDs; n = 5; **p < 0.01 by Student's t test.

(E) Percentage of CD41^{+} cells after 3-day culture of HSCs with or without KPT-330. Means ± SDs; n = 5; **p < 0.01 by Student's t test.

(F) Mk colony assay of 750 HSCs obtained from KPT-330 (−) or (+) culture. Means ± SDs; n = 4; **p < 0.01 by Student's t test.

(G) Representative flow cytometry plots and MFI of pSTAT3 (S727) on HSCs obtained from treated with PBS (control) or romiplostim (Romi). Means ± SDs; n = 4; *p < 0.05 by Student's t test.

(H) MFI of pSTAT3 (S727) on TMRE^{hi} or TMRE^{lo} HSCs. Means ± SDs; n = 5; ns, not significant by Student's t test.

(I) MFI of pSTAT3 (S727) on TMRE^{hi} or TMRE^{lo} HSCs cultured for 3 days in Thpo containing medium. Means ± SDs; n = 5; *p < 0.05 by Student's t test.

(J) Representative image of pSTAT3 (S727) localization in mitochondria in MTG^{hi} (Mito^{hi}) and MTG^{lo} (Mito^{lo}) cells. TOMM20 (green) stained for mitochondria along with pSTAT3 (S727) (red). Dotted lines represent the location of the cell membrane. Scale bar, 2 μm (upper) and 0.2 μm (lower).

(K) Relative expression of GRIM-19 (Ndufa13) gene to *B2m* expression in TMRE^{hi} or TMRE^{lo} HSCs. Means ± SDs; n = 4; *p < 0.05 by Student's t test.

(L) MFI of GRIM-19 on MitoTracker Red^{hi} (Mito^{hi}) or MitoTracker Red^{lo} (Mito^{lo}) HSCs. Means ± SDs; n = 5; *p < 0.05 by Student's t test.

and active during stress hematopoiesis. Furthermore, we have unpublished data showing that mitochondrial metabolism in neonatal HSCs, which are highly proliferative, differs from that of adult HSCs. Therefore, HSCs are likely heterogeneous in terms of metabolic state, particularly in terms of mitochondrial activity. Such metabolic heterogeneity may be relevant to the platelet reconstitution potential of human HSCs in BM transplantation from different donors.

Recent advances in single-cell-based analyses support HSC heterogeneity and confirm that a hallmark of such heterogeneity is preferential differentiation to an Mk-lineage. Others have identified some HSC subpopulations that retain long-term

repopulation potential but preferentially differentiate along the Mk-lineage (Pronk et al., 2007; Shin et al., 2014; Sanjuan-Pla et al., 2013; Carrelha et al., 2018). Our transplantation of small numbers of HSCs (Figure 3C) revealed that mitochondrial activity is positively correlated with myeloid-biased differentiation. Furthermore, we found that HSCs from Thpo$^{-/-}$ mice exhibit significantly lower mitochondrial activity than those from WT mice, supporting the idea that Thpo signaling functions in the maintenance of mitochondria-active HSCs.

HSCs purified with flow cytometry based on surface marker expression may be restricted to Mk-lineage differentiation (Yamamoto et al., 2013). CD41^{high} HSC subsets have been identified as Mk-committed progenitor cells during inflammatory stress (Haas et al., 2015). CD41^{high} HSCs rapidly expand to compensate for thrombocytopenia in a mouse inflammation model using polyinosinic:polycytidylic acid (pIpC). While mitochondria-active HSCs show myeloid bias in unperturbed hematopoiesis, our data indicate that Thpo-activated HSCs show mitochondrial activation but are not Mk biased because they do not exhibit robust multilineage long-term reconstitution (Figure 1D). In fact, because Thpo stimulation rapidly decreases HSC number and stem cell potential but increases Mk-lineage output of the stem cell pool, Thpo may accelerate the formation of Mk-biased progenitors. Thpo signaling did upregulate CD41 expression in HSCs (Figure 4A). pIpC-induced IFN signaling modulates protein synthesis in a manner that subsequently activates Mk-biased progenitors, resulting in rapid Mk and platelet formation (Haas et al., 2015). We provide data showing that HSC Mk-lineage differentiation is stimulated by Thpo-dependent mitochondrial activation. However, it remains unclear whether steady-state, Mk-biased, mitochondria-rich HSCs directly give rise to Mk-committed progenitors in stress conditions. Nevertheless, our observations provide strong evidence that a high energy profile requiring mitochondrial activity shifts HSCs toward an Mk-lineage. Others report that mitochondrial biosynthesis induced by non-invasive low-level laser therapy enhances Mk maturation and platelet formation (Zhang et al., 2016). Further understanding of mitochondrial metabolic pathways may provide methods useful to manipulate HSCs *in vivo* to treat thrombocytopenia and *ex vivo* to produce transplantable platelets.

Among the Mk cell surface markers, we found that expression of the tetraspanin CD9 was positively correlated with HSC mitochondrial activity. CD9 has been used as a marker to identify MkP, and it also regulates activities including cell fusion, migration, and morphogenesis in various cell contexts (Hemler, 2005; Iwasaki et al., 2013; Suzuki et al., 2009). However, the function of CD9 on MkPs during Mk differentiation and whether CD9 deficiency perturbs adult hematopoiesis are not known. Here, we used CD9 solely as a cell surface marker to identify Mk-HSCs. Its function in Mk-biased hematopoiesis should be addressed in future studies.

pSTAT translocation to mitochondria reportedly enhances metabolism in cells of various tissues or in cancer cells, including T cell leukemia cells (Wegrzyn et al., 2009; Chueh et al., 2010). Mitochondrial STAT translocation is implicated in cell turnover, especially in cardiac tissue, where mitochondrial STAT3 activates complexes I, II, and V of the electron transport system; improves complex I respiratory activity and calcium retention; and inhibits apoptosis by blocking mitochondrial permeability transition pore (MPTP)-mediated cytochrome *c* release (Boengler et al., 2010; Heusch et al., 2011). Nevertheless, we suspect that multiple signaling pathways, including the nuclear effect of pSTAT3, stimulate *de novo* energy generation and may be activated during Mk-lineage differentiation. Ultimately, STAT translocation may be manipulated to enhance HSC mitochondrial metabolism. Moreover, our observations encourage future analysis of the role played by mitochondrial STAT translocation in hematopoietic disease involving abnormal Mks, such as myeloproliferative diseases or acute megakaryocytic leukemia (Papadantonakis et al., 2012).

In conclusion, we show that HSCs are heterogeneous metabolically and that, during steady-state hematopoiesis, they are primed toward Mk-lineage differentiation when mitochondrial content is elevated. Thpo rapidly stimulated mitochondrial activation and Mk-lineage differentiation during stress hematopoiesis. Our study provides evidence that the stem cell metabolic state is a factor in both multipotency and cell fate determination. Our work provides insight into Thpo function, suggests that metabolic regulators could be useful to treat pathologies marked by abnormal Mks, and sheds light on how HSCs could be manipulated to generate transplantable platelets.

STAR★METHODS

Detailed methods are provided in the online version of this paper and include the following:

- KEY RESOURCES TABLE
- CONTACT FOR REAGENT AND RESOURCE SHARING
- EXPERIMENTAL MODEL AND SUBJECT DETAILS
  - Animal models
- METHOD DETAILS
  - Flow cytometric analysis
  - BM Transplantation
  - *In vitro* HSC and Mk cultures
  - *In vivo* assays
  - Quantitative PCR assay
  - Seahorse analysis
  - RNA sequencing and gene set enrichment analysis
  - Transmission Electron microscopy
  - Confocal microscopy and quantification of fluorescent images
  - Super-resolution imaging
  - Mass cytometry
- QUANTIFICATION AND STATISTICAL ANALYSIS
  - Single cell RNA sequencing analysis
  - Gene-set and gene-ontology enrichment analyses
  - Mass Cytometry data analysis
  - Statistical analysis
- DATA AND SOFTWARE AVAILABILITY

SUPPLEMENTAL INFORMATION

Supplemental Information includes six figures and can be found with this article online at https://doi.org/10.1016/j.celrep.2018.10.059.

ACKNOWLEDGMENTS

The authors thank Mr. Akifumi Kiyota and Ms. Ryoko Koitabashi at the International Research Center for Medical Sciences (IRCMS), Kumamoto University, for technical assistance in the CyTOF experiments. This study was supported by the National Medical Research Council (NMRC) Grant of Singapore Translational Research Investigator Award (NMRC/STaR/0019/2014 to T.S.), the KAKEN Grant-in-Aid for Scientific Research (S) (26221309 to T.S.), the NMRC Clinician Scientist-Individual Research Grant (CS-IRG) New Investigator Grant (NMRC/CNIG/1164/2017 to A.N.-I.), the KAKEN Grant-in-Aid for Young Scientists (A) (26713035 to A.N.-I.), the KAKEN Grant-in-Aid for Scientific Research (C) (18K08364 to A.N.-I.), and the KAKEN Fund for the Promotion of Joint International Research (Fostering Joint International Research) (15KK0350 to A.N.-I.).

AUTHOR CONTRIBUTIONS

T.S. and A.N.-I. designed the project, analyzed the data, and wrote the manuscript. A.N.-I. organized, performed, and analyzed all of the experiments. T.U., T.M., Y.T., and H.T. discussed, performed, and analyzed some experiments. A.B.B.A.M. assisted in performing experiments. A.O. developed the Thpo$^{-/-}$ mice. T.M., P.S.S., and B.D.M. discussed and analyzed the single-cell sequence and CyTOF data. All of the authors read and approved the final manuscript.

DECLARATION OF INTERESTS

The authors declare no competing interests.

Received: July 28, 2017
Revised: September 7, 2018
Accepted: October 15, 2018
Published: November 13, 2018

REFERENCES

Ansó, E., Weinberg, S.E., Diebold, L.P., Thompson, B.J., Malinge, S., Schumacker, P.T., Liu, X., Zhang, Y., Shao, Z., Steadman, M., et al. (2017). The mitochondrial respiratory chain is essential for haematopoietic stem cell function. Nat. Cell Biol. *19*, 614–625.

Boengler, K., Hilfiker-Kleiner, D., Heusch, G., and Schulz, R. (2010). Inhibition of permeability transition pore opening by mitochondrial STAT3 and its role in myocardial ischemia/reperfusion. Basic Res. Cardiol. *105*, 771–785.

Burkewitz, K., Zhang, Y., and Mair, W.B. (2014). AMPK at the nexus of energetics and aging. Cell Metab. *20*, 10–25.

Carrelha, J., Meng, Y., Kettyle, L.M., Luis, T.C., Norfo, R., Alcolea, V., Boukarabila, H., Grasso, F., Gambardella, A., Grover, A., et al. (2018). Hierarchically related lineage-restricted fates of multipotent haematopoietic stem cells. Nature *554*, 106–111.

Ceresa, I.F., Noris, P., Ambaglio, C., Pecci, A., and Balduini, C.L. (2007). Thrombopoietin is not uniquely responsible for thrombocytosis in inflammatory disorders. Platelets *18*, 579–582.

Cerutti, A., Custodi, P., Mduranti, Cazzola, M., and Balduini, C.L. (1999). Circulating thrombopoietin in reactive conditions behaves like an acute phase reactant. Clin. Lab. Haematol. *21*, 271–275.

Chen, S., Su, Y., and Wang, J. (2013). ROS-mediated platelet generation: a microenvironment-dependent manner for megakaryocyte proliferation, differentiation, and maturation. Cell Death Dis. *4*, e722.

Chueh, F.-Y., Leong, K.-F., and Yu, C.-L. (2010). Mitochondrial translocation of signal transducer and activator of transcription 5 (STAT5) in leukemic T cells and cytokine-stimulated cells. Biochem. Biophys. Res. Commun. *402*, 778–783.

Crisan, M., and Dzierzak, E. (2016). The many faces of hematopoietic stem cell heterogeneity. Development *143*, 4571–4581.

Croker, B.A., Silke, J., and Gerlic, M. (2015). Fight or flight: regulation of emergency hematopoiesis by pyroptosis and necroptosis. Curr. Opin. Hematol. *22*, 293–301.

Dani, A., Huang, B., Bergan, J., Dulac, C., and Zhuang, X. (2010). Superresolution imaging of chemical synapses in the brain. Neuron *68*, 843–856.

de Almeida, M.J., Luchsinger, L.L., Corrigan, D.J., Williams, L.J., and Snoeck, H.-W. (2017). Dye-independent methods reveal elevated mitochondrial mass in hematopoietic stem cells. Cell Stem Cell *21*, 725–729.e4.

Forsberg, E.C., Prohaska, S.S., Katzman, S., Heffner, G.C., Stuart, J.M., and Weissman, I.L. (2005). Differential expression of novel potential regulators in hematopoietic stem cells. PLoS Genet. *1*, e28.

Gekas, C., and Graf, T. (2013). CD41 expression marks myeloid-biased adult hematopoietic stem cells and increases with age. Blood *121*, 4463–4472.

Grinenko, T., Arndt, K., Portz, M., Mende, N., Günther, M., Cosgun, K.N., Alexopoulou, D., Lakshmanaperumal, N., Henry, I., Dahl, A., and Waskow, C. (2014). Clonal expansion capacity defines two consecutive developmental stages of long-term hematopoietic stem cells. J. Exp. Med. *211*, 209–215.

Guimarães, E.L., Best, J., Dollé, L., Najimi, M., Sokal, E., and van Grunsven, L.A. (2012). Mitochondrial uncouplers inhibit hepatic stellate cell activation. BMC Gastroenterol. *12*, 68.

Gurney, A.L., Carver-Moore, K., de Sauvage, F.J., and Moore, M.W. (1994). Thrombocytopenia in c-mpl-deficient mice. Science *265*, 1445–1447.

Haas, S., Hansson, J., Klimmeck, D., Loeffler, D., Velten, L., Uckelmann, H., Wurzer, S., Prendergast, Á.M., Schnell, A., Hexel, K., et al. (2015). Inflammation-induced emergency megakaryopoiesis driven by hematopoietic stem cell-like megakaryocyte progenitors. Cell Stem Cell *17*, 422–434.

Hemler, M.E. (2005). Tetraspanin functions and associated microdomains. Nat. Rev. Mol. Cell Biol. *6*, 801–811.

Heusch, G., Musiolik, J., Gedik, N., and Skyschally, A. (2011). Mitochondrial STAT3 activation and cardioprotection by ischemic postconditioning in pigs with regional myocardial ischemia/reperfusion. Circ. Res. *109*, 1302–1308.

Iwasaki, T., Takeda, Y., Maruyama, K., Yokosaki, Y., Tsujino, K., Tetsumoto, S., Kuhara, H., Nakanishi, K., Otani, Y., Jin, Y., et al. (2013). Deletion of tetraspanin CD9 diminishes lymphangiogenesis in vivo and in vitro. J. Biol. Chem. *288*, 2118–2131.

Kabaya, K., Akahori, H., Shibuya, K., Nitta, Y., Ida, M., Kusaka, M., Kato, T., and Miyazaki, H. (1996). In vivo effects of pegylated recombinant human megakaryocyte growth and development factor on hematopoiesis in normal mice. Stem Cells *14*, 651–660.

Kaushansky, K. (2016). Thrombopoietin and its receptor in normal and neoplastic hematopoiesis. Thromb. J. *14* (*Suppl 1*), 40.

Kovtonyuk, L.V., Manz, M.G., and Takizawa, H. (2016). Enhanced thrombopoietin but not G-CSF receptor stimulation induces self-renewing hematopoietic stem cell divisions in vivo. Blood *127*, 3175–3179.

Kramer, A.H., Kadye, R., Houseman, P.S., and Prinsloo, E. (2015). Mitochondrial STAT3 and reactive oxygen species: a fulcrum of adipogenesis? JAK-STAT *4*, e1084084.

Kumar, S., Ciraolo, G., Hinge, A., and Filippi, M.-D. (2014). An efficient and reproducible process for transmission electron microscopy (TEM) of rare cell populations. J. Immunol. Methods *404*, 87–90.

Langmead, B., and Salzberg, S.L. (2012). Fast gapped-read alignment with Bowtie 2. Nat. Methods *9*, 357–359.

Léon, C., Evert, K., Dombrowski, F., Pertuy, F., Eckly, A., Laeuffer, P., Gachet, C., and Greinacher, A. (2012). Romiplostim administration shows reduced megakaryocyte response-capacity and increased myelofibrosis in a mouse model of MYH9-RD. Blood *119*, 3333–3341.

Li, X., and Slayton, W.B. (2013). Molecular mechanisms of platelet and stem cell rebound after 5-fluorouracil treatment. Exp. Hematol. *41*, 635–645.e3.

Liu, X., Zhang, Y., Ni, M., Cao, H., Signer, R.A.J., Li, D., Li, M., Gu, Z., Hu, Z., Dickerson, K.E., et al. (2017). Regulation of mitochondrial biogenesis in erythropoiesis by mTORC1-mediated protein translation. Nat. Cell Biol. *19*, 626–638.

Luchsinger, L.L., de Almeida, M.J., Corrigan, D.J., Mumau, M., and Snoeck, H.-W. (2016). Mitofusin 2 maintains haematopoietic stem cells with extensive lymphoid potential. Nature *529*, 528–531.

Machlus, K.R., Wu, S.K., Vijey, P., Soussou, T.S., Liu, Z.-J., Shacham, E., Unger, T.J., Kashyap, T., Klebanov, B., Sola-Visner, M., et al. (2017). Selinexor-induced thrombocytopenia results from inhibition of thrombopoietin signaling in early megakaryopoiesis. Blood *130*, 1132–1143.

Mantel, C., Messina-Graham, S., and Broxmeyer, H.E. (2010). Upregulation of nascent mitochondrial biogenesis in mouse hematopoietic stem cells parallels upregulation of CD34 and loss of pluripotency: a potential strategy for reducing oxidative risk in stem cells. Cell Cycle *9*, 2008–2017.

Meier, J.A., and Larner, A.C. (2014). Toward a new STATe: the role of STATs in mitochondrial function. Semin. Immunol. *26*, 20–28.

Mi, H., Huang, X., Muruganujan, A., Tang, H., Mills, C., Kang, D., and Thomas, P.D. (2017). PANTHER version 11: expanded annotation data from Gene Ontology and Reactome pathways, and data analysis tool enhancements. Nucleic Acids Res. *45* (*D1*), D183–D189.

Mihaylova, M.M., and Shaw, R.J. (2011). The AMPK signalling pathway coordinates cell growth, autophagy and metabolism. Nat. Cell Biol. *13*, 1016–1023.

Mootha, V.K., Lindgren, C.M., Eriksson, K.-F., Subramanian, A., Sihag, S., Lehar, J., Puigserver, P., Carlsson, E., Ridderstråle, M., Laurila, E., et al. (2003). PGC-1α-responsive genes involved in oxidative phosphorylation are coordinately downregulated in human diabetes. Nat. Genet. *34*, 267–273.

Mortensen, M., Soilleux, E.J., Djordjevic, G., Tripp, R., Lutteropp, M., Sadighi-Akha, E., Stranks, A.J., Glanville, J., Knight, S., Jacobsen, S.-E.W., et al. (2011). The autophagy protein Atg7 is essential for hematopoietic stem cell maintenance. J. Exp. Med. *208*, 455–467.

Nakamura-Ishizu, A., Morikawa, S., Shimizu, K., and Ezaki, T. (2008). Characterization of sinusoidal endothelial cells of the liver and bone marrow using an intravital lectin injection method. J. Mol. Histol. *39*, 471–479.

Nakamura-Ishizu, A., Okuno, Y., Omatsu, Y., Okabe, K., Morimoto, J., Uede, T., Nagasawa, T., Suda, T., and Kubota, Y. (2012). Extracellular matrix protein tenascin-C is required in the bone marrow microenvironment primed for hematopoietic regeneration. Blood *119*, 5429–5437.

Nakamura-Ishizu, A., Takizawa, H., and Suda, T. (2014). The analysis, roles and regulation of quiescence in hematopoietic stem cells. Development *141*, 4656–4666.

Notta, F., Zandi, S., Takayama, N., Dobson, S., Gan, O.I., Wilson, G., Kaufmann, K.B., McLeod, J., Laurenti, E., Dunant, C.F., et al. (2016). Distinct routes of lineage development reshape the human blood hierarchy across ontogeny. Science *351*, aab2116.

Oguro, H., Ding, L., and Morrison, S.J. (2013). SLAM family markers resolve functionally distinct subpopulations of hematopoietic stem cells and multipotent progenitors. Cell Stem Cell *13*, 102–116.

Ott, M., Gogvadze, V., Orrenius, S., and Zhivotovsky, B. (2007). Mitochondria, oxidative stress and cell death. Apoptosis *12*, 913–922.

Papadantonakis, N., Matsuura, S., and Ravid, K. (2012). Megakaryocyte pathology and bone marrow fibrosis: the lysyl oxidase connection. Blood *120*, 1774–1781.

Petit, I., Szyper-Kravitz, M., Nagler, A., Lahav, M., Peled, A., Habler, L., Ponomaryov, T., Taichman, R.S., Arenzana-Seisdedos, F., Fujii, N., et al. (2002). G-CSF induces stem cell mobilization by decreasing bone marrow SDF-1 and up-regulating CXCR4. Nat. Immunol. *3*, 687–694.

Piccoli, C., Ria, R., Scrima, R., Cela, O., D'Aprile, A., Boffoli, D., Falzetti, F., Tabilio, A., and Capitanio, N. (2005). Characterization of mitochondrial and extramitochondrial oxygen consuming reactions in human hematopoietic stem cells. Novel evidence of the occurrence of NAD(P)H oxidase activity. J. Biol. Chem. *280*, 26467–26476.

Pronk, C.J.H., Rossi, D.J., Månsson, R., Attema, J.L., Norddahl, G.L., Chan, C.K.F., Sigvardsson, M., Weissman, I.L., and Bryder, D. (2007). Elucidation of the phenotypic, functional, and molecular topography of a myeloerythroid progenitor cell hierarchy. Cell Stem Cell *1*, 428–442.

Qian, H., Buza-Vidas, N., Hyland, C.D., Jensen, C.T., Antonchuk, J., Månsson, R., Thoren, L.A., Ekblom, M., Alexander, W.S., and Jacobsen, S.E. (2007). Critical role of thrombopoietin in maintaining adult quiescent hematopoietic stem cells. Cell Stem Cell *1*, 671–684.

Ruscetti, F.W., and Bartelmez, S.H. (2001). Transforming growth factor beta, pleiotropic regulator of hematopoietic stem cells: potential physiological and clinical relevance. Int. J. Hematol. *74*, 18–25.

Sakaue-Sawano, A., Kurokawa, H., Morimura, T., Hanyu, A., Hama, H., Osawa, H., Kashiwagi, S., Fukami, K., Miyata, T., Miyoshi, H., et al. (2008). Visualizing spatiotemporal dynamics of multicellular cell-cycle progression. Cell *132*, 487–498.

Sanjuan-Pla, A., Macaulay, I.C., Jensen, C.T., Woll, P.S., Luis, T.C., Mead, A., Moore, S., Carella, C., Matsuoka, S., Bouriez Jones, T., et al. (2013). Platelet-biased stem cells reside at the apex of the haematopoietic stem-cell hierarchy. Nature *502*, 232–236.

Schaefer, B.C., Schaefer, M.L., Kappler, J.W., Marrack, P., and Kedl, R.M. (2001). Observation of antigen-dependent CD8+ T-cell/ dendritic cell interactions in vivo. Cell. Immunol. *214*, 110–122.

Shin, J.Y., Hu, W., Naramura, M., and Park, C.Y. (2014). High c-kit expression identifies hematopoietic stem cells with impaired self-renewal and megakaryocytic bias. J. Exp. Med. *211*, 217–231.

Simsek, T., Kocabas, F., Zheng, J., Deberardinis, R.J., Mahmoud, A.I., Olson, E.N., Schneider, J.W., Zhang, C.C., and Sadek, H.A. (2010). The distinct metabolic profile of hematopoietic stem cells reflects their location in a hypoxic niche. Cell Stem Cell *7*, 380–390.

Spencer, J.A., Ferraro, F., Roussakis, E., Klein, A., Wu, J., Runnels, J.M., Zaher, W., Mortensen, L.J., Alt, C., Turcotte, R., et al. (2014). Direct measurement of local oxygen concentration in the bone marrow of live animals. Nature *508*, 269–273.

Stetler, R.A., Leak, R.K., Yin, W., Zhang, L., Wang, S., Gao, Y., and Chen, J. (2012). Mitochondrial biogenesis contributes to ischemic neuroprotection afforded by LPS pre-conditioning. J. Neurochem. *123* (*Suppl 2*), 125–137.

Subramanian, A., Tamayo, P., Mootha, V.K., Mukherjee, S., Ebert, B.L., Gillette, M.A., Paulovich, A., Pomeroy, S.L., Golub, T.R., Lander, E.S., and Mesirov, J.P. (2005). Gene set enrichment analysis: a knowledge-based approach for interpreting genome-wide expression profiles. Proc. Natl. Acad. Sci. USA *102*, 15545–15550.

Suzuki, M., Tachibana, I., Takeda, Y., He, P., Minami, S., Iwasaki, T., Kida, H., Goya, S., Kijima, T., Yoshida, M., et al. (2009). Tetraspanin CD9 negatively regulates lipopolysaccharide-induced macrophage activation and lung inflammation. J. Immunol. *182*, 6485–6493.

Takubo, K., Goda, N., Yamada, W., Iriuchishima, H., Ikeda, E., Kubota, Y., Shima, H., Johnson, R.S., Hirao, A., Suematsu, M., and Suda, T. (2010). Regulation of the HIF-1alpha level is essential for hematopoietic stem cells. Cell Stem Cell *7*, 391–402.

Tammineni, P., Anugula, C., Mohammed, F., Anjaneyulu, M., Larner, A.C., and Sepuri, N.B.V. (2013). The import of the transcription factor STAT3 into mitochondria depends on GRIM-19, a component of the electron transport chain. J. Biol. Chem. *288*, 4723–4732.

Tomura, M., Sakaue-Sawano, A., Mori, Y., Takase-Utsugi, M., Hata, A., Ohtawa, K., Kanagawa, O., and Miyawaki, A. (2013). Contrasting quiescent G0 phase with mitotic cell cycling in the mouse immune system. PLoS One *8*, e73801.

Trapnell, C., Hendrickson, D.G., Sauvageau, M., Goff, L., Rinn, J.L., and Pachter, L. (2013). Differential analysis of gene regulation at transcript resolution with RNA-seq. Nat. Biotechnol. *31*, 46–53.

van der Maaten, L., and Hinton, G. (2008). Visualizing data using t-SNE. J. Mach. Learn. Res. *9*, 2579–2605.

Vannini, N., Girotra, M., Naveiras, O., Nikitin, G., Campos, V., Giger, S., Roch, A., Auwerx, J., and Lutolf, M.P. (2016). Specification of haematopoietic stem cell fate via modulation of mitochondrial activity. Nat. Commun. *7*, 13125.

Walter, D., Lier, A., Geiselhart, A., Thalheimer, F.B., Huntscha, S., Sobotta, M.C., Moehrle, B., Brocks, D., Bayindir, I., Kaschutnig, P., et al. (2015). Exit from dormancy provokes DNA-damage-induced attrition in haematopoietic stem cells. Nature *520*, 549–552.

Wegrzyn, J., Potla, R., Chwae, Y.J., Sepuri, N.B., Zhang, Q., Koeck, T., Derecka, M., Szczepanek, K., Szelag, M., Gornicka, A., et al. (2009). Function of mitochondrial Stat3 in cellular respiration. Science *323*, 793–797.

Woolthuis, C.M., and Park, C.Y. (2016). Hematopoietic stem/progenitor cell commitment to the megakaryocyte lineage. Blood *127*, 1242–1248.

Yamamoto, R., Morita, Y., Ooehara, J., Hamanaka, S., Onodera, M., Rudolph, K.L., Ema, H., and Nakauchi, H. (2013). Clonal analysis unveils self-renewing lineage-restricted progenitors generated directly from hematopoietic stem cells. Cell *154*, 1112–1126.

Yoshihara, H., Arai, F., Hosokawa, K., Hagiwara, T., Takubo, K., Nakamura, Y., Gomei, Y., Iwasaki, H., Matsuoka, S., Miyamoto, K., et al. (2007). Thrombopoietin/MPL signaling regulates hematopoietic stem cell quiescence and interaction with the osteoblastic niche. Cell Stem Cell *1*, 685–697.

Zhang, Q., Dong, T., Li, P., and Wu, M.X. (2016). Noninvasive low-level laser therapy for thrombocytopenia. Sci. Transl. Med. *8*, 349ra101.

STAR★METHODS

KEY RESOURCES TABLE

REAGENT or RESOURCE	SOURCE	IDENTIFIER
Antibodies		
CD16/32 [93]	eBioscience / Biolegend	14-0161 / 101320; RRID: AB_312800/AB_467132
CD16/32 [93], AF700	eBioscience	56-0161-82; RRID: AB_493994
CD4 [RM4-5], PerCp-Cy5.5	Biolegend	100540; RRID: AB_2563022
CD8a [53-6.7], PerCp-Cy5.5	Biolegend	100734; RRID: AB_893427
Gr-1 [RB6-8C5], PerCp-Cy5.5	Biolegend	108428; RRID: AB_893561
Mac-1 [M1/70], PerCp-Cy5.5	Biolegend	101228; RRID: AB_893233
B220 [RA3-6B2], PerCp-Cy5.5	Biolegend	103236; RRID: AB_893356
Ter-119 [TER-119], PerCp-Cy5.5	Biolegend	116228; RRID: AB_893638
c-Kit [2B8], APC-Cy7	Biolegend	105826; RRID: AB_1626280
Sca-1 [D7], PE-Cy7	Biolegend	108114; RIID: AB_493597
Sca-1 [D7], APC-Cy7	Biolegend	108126; RRID: AB_10639725
CD150 [TC15-12F12.2], APC	Biolegend	115910; RRID: AB_493461
CD150 [TC15-12F12.2], PE	Biolegend	115904; RRID: AB_313682
CD150 [TC15-12F12.2], PEcy7	Biolegend	115914; RRID: AB_439796
CD48 [HM48-1], AF700	Biolegend	103426; RRID: AB_10612754
CD45.1 [A20], PE	Biolegend	110708; RRID: AB_313496
CD45.1 [A20], AF700	Biolegend	110724; RRID: AB_493732
CD45.2 [104], APC-Cy7	Biolegend	109824; RRID: AB_830788
CD8a [53-6.7], PE-Cy7	Biolegend	100722; RRID: AB_312760
Gr-1 [RB6-8C5], APC	BD	553129; RRID: AB_2314614
Mac-1 [M1/70], APC	Biolegend	101212; RRID: AB_312794
B220 [RA3-6B2], PECy7	BD	552772; RRID: AB_394458
c-Kit [2B8], BV421	Biolegend	105828; RRID: AB_10898120
Flt-3 [A2F10.1], APC	eBioscience	17-1351-80; RRID: AB_10596653
Flt-3 [A2F10.1], PE	Biolegend	135305; RRID: AB_1877217
CD41 [MWReg30], PE	BD	558040; RRID: AB_397004
CD41 [MWReg30], APC	Invitrogen	17-0411-82; RRID: AB_1603238
IL-7Rα [A7R34], PE	eBioscience	12-1271-81; RRID: AB_465845
IL-7Rα [A7R34], BV510	Biolegend	135033; RRID: AB_2564576
Endoglin [MJ7/18]	Biolegend	120410; RRID: AB_1027702
CD9 [KMC8], BV421	BD Horizon	564235; RRID: AB_395032
CD34 [RAM34], FITC	eBioscience	11-034-85; RRID: AB_465020
Mpl [AMM2], Biotin	IBL	10403
Ki67 [SolA15], PE	eBioscience	12-5698-82; RRID: AB_11150954
AnnexinV, PE	Life Technologies	A35111
pSTAT3 (S727)[49]	BD Phosflow	558557
GRIM19 [6E1BH7]	Abcam	ab110240; RRID: AB_303811
TOMM20	Abcam	Ab186734; RRID: AB_2043078
pAMPKα (Thr172) [40H9]	CST	2535; RRID: AB_331250
CD41-143Nd [MWreg30]	Fluidigm	3143009B
SOCS3 [516919]	R&D	MAB5696; RRID: AB_2193299
pStat5 (Y694)-147Sm [47]	Fluidigm	3147012A
SOCS1 [4H1]	ThermoScientific	37-4100; RRID: AB_10890785

(*Continued on next page*)

Continued

REAGENT or RESOURCE	SOURCE	IDENTIFIER
anti-biotin-150Nd	Fluidigm	3150008B
pAkt (S473) −152Sm [D9E]	Fluidigm	3152005A
pStat1 (Y701)- 153Eu [58D6]	Fluidigm	3153003A
CD48-154Sm [HM48-1]	Fluidigm	3154004B
p38 (T180/Y182)- 156Gd [D3F9]	Fluidigm	3156002A
pStat3 (Y705)- 158Gd [4]	Fluidigm	3158005A
pMAPKAPK2 (T334)- 159Tb [27B7]	Fluidigm	3159010A
pJak2 (Tyr1008) [D4A8]	CST	8082S; RRID: AB_10949104
Tie2 [TEK4]	Biolegend	124002; RRID: AB_961175
mTOR (phospho S2448) [EPR426(2)]	Abcam	ab109268; RRID: AB_297588
EPCR [eBio1560]	eBioscience	16-2012-83; RRID: AB_657692
CD150 −167Er [TC15-12F12.2]	Fluidigm	3167004B
CD61 [2C9.G2]	Biolegend	104302; RRID: AB_313079
Ly-6A/E (Sca-1)- 169Tm [D7]	Fluidigm	3169015B
pERK 1/2 (T202/Y204)- 171Yb [D13.14.4E]	Fluidigm	3171010A
CD117 (ckit)- 173Yb [2B8]	Fluidigm	3173004B
pStat3 (S727) [ab30647]	Abcam	ab86430; RRID: AB_779085
Pgc1a	Abcam	ab54481; RRID: AB_881987
Chemicals, Peptides, and Recombinant Proteins		
Romiplostim	Kyowa Kirin	n/a
MitotrackerTM Green FM	ThermoScientific	M7514
TMRE	Enzo	52309
CellROX	ThermoScientific	C10448
recombinant human Thpo (PEG-rHuMGDF)	Kyowa Kirin	n/a
Filgrastim	Kyowa Kirin	n/a
antimycin	Sigma	A8674
rotenone	Abcam	ab143145
oligomycin	Abcam	ab141829
FCCP	Abcam	ab120081
KPT-330	Cayman chemical	18127
murine recombinant SCF	Peprotech	250-03
murine recombinant Thpo	Peprotech	315-14
cisplatin (Cell-ID Cisplatin)	Fluidigm	201198
Critical Commercial Assays		
CellTiter-Glo® 2.0 Assay kit	Promega	G9241
MegaCult	Stem cell Technologies	04960
MethoCult	Stem cell Technologies	M3234
LIVE/DEAD Viability/cytotoxicity Kit	Life Technologies	MP03224
SMARTer Ultra Low RNA Kit for Fluidigm C1 system	Clonetech	634936
Illumina Nextera XT DNA Sample Preparation Kit	Illumina	FC-131-1096/FC-131-1002
C1 Single-cell Auto Prep Reagent kit for mRNA-seq	Fluidigm	100-6201
Superscript VILO	Invitrogen	11754250
RNeasy Mini Kit	QIAGEN	74106
IntraPrep reagents	Beckman Coulter	IM2389
Maxpar antibody labeling kit	Fluidigm	201300
MaxPar Fix I buffer	Fluidigm	201065
Maxpar® Cell Staining Buffer	Fluidigm	201068
Cell-ID Intercalator-Ir	Fluidigm	201192A
Maxpar® Fix and Perm Buffer	Fluidigm	201057

(*Continued on next page*)

Continued

REAGENT or RESOURCE	SOURCE	IDENTIFIER
Deposited Data		
RNA-seq: Thrombopoietin metabolically primes hematopoietic stem cells to megakaryocyte lineage differentiation	This paper	GEO: GSE121001
Experimental Models: Organisms/Strains		
Mouse: Thpo−/−	Toshio Suda Lab	n/a
Mouse: UBC-GFP (C57BL/6-Tg(UBC-GFP)30Scha/J)	Jackson laboratory	004353
Mouse: CD45.1	Jackson laboratory	002014
Mouse: Mito-Dendra2 (Gt(ROSA)26Sortm1.1(CAG-COX8A/Dendra2)Dcc)	Jackson laboratory	018385
Mouse: (Fucci) GMNN-mAG mice (B6.Cg-Tg(FucciS/G2/M)#474Bsi	RIKEN	RBRC02704
Oligonucleotides		
Taqman primer: Ppargc1a	Thermo Fisher Scientific	Mm01208835_m1
Taqman primer: Tfam	Thermo Fisher Scientific	Mm00447485_m1
Taqman primer: Nrf1	Thermo Fisher Scientific	Mm01135606_m1
Taqman primer: Sdhb	Thermo Fisher Scientific	Mm00458272_m1
Taqman primer: Sdhc	Thermo Fisher Scientific	Mm00481172_m1
Taqman primer: Atp5a	Thermo Fisher Scientific	Mm00431960_m1
Taqman primer: Cox5a	Thermo Fisher Scientific	Mm00432638_m1
Taqman primer: Cyc1	Thermo Fisher Scientific	Mm00470540_m1
Taqman primer: Ndufa13	Thermo Fisher Scientific	Mm00445751_m1
Taqman primer: B2m	Thermo Fisher Scientific	Mm03003532_u1
Taqman primer: Bax	Thermo Fisher Scientific	Mm00432051_m1
Taqman primer: Bak1	Thermo Fisher Scientific	Mm00432045_m1
Taqman primer: Bcl2	Thermo Fisher Scientific	Mm00477631_m1
Taqman primer: Prdx1	Thermo Fisher Scientific	Mm01621996_s1
Taqman primer: Prdx3	Thermo Fisher Scientific	Mm00545848_m1
Taqman primer: Gpx1	Thermo Fisher Scientific	Mm00656767_g1
Taqman primer: Gpx4	Thermo Fisher Scientific	Mm00515041_m1
Taqman primer: Txn2	Thermo Fisher Scientific	Mm00444931_m1
Software and Algorithms		
FlowJo 10.1	Tree Star	n/a
QuantStudioTM Design and Analysis Software 1.3.1	Thermo Fisher Scientific	n/a
Agilent Seahorse Wave Desktop	Agilent	n/a
R	R Foundation	version 3.3.2
Rtsne package		version 0.13
Cufflinks		version 2.2.1
PANTHER		release 20160715
GSEA	Broad institute	Version 2.0.13
NIS elements	Nikon	n/a
ImageJ		n/a
Cytobank.		n/a
flowCore		n/a
flowViz		n/a
flowUtils		n/a

CONTACT FOR REAGENT AND RESOURCE SHARING

Further information and requests for resources and reagents should be directed to and will be fulfilled by the Lead Contact, Toshio Suda (sudato@keio.jp).

EXPERIMENTAL MODEL AND SUBJECT DETAILS

Animal models

All mice were on a C57BL/6N background. C57BL/6-Ly5.1 mice were used for competitive repopulation assays. Fucci Tg mice (GMNN-mAG mice (B6.Cg-Tg(FucciS/G2/M)#474Bsi)) were obtained from RIKEN (Sakaue-Sawano et al., 2008)(Tomura et al., 2013). UBC-GFP (C57BL/6-Tg(UBC-GFP)30Scha/J) mice and Mito-Dendra2 transgenic (Gt(ROSA)26Sortm1.1(CAG-COX8A/Dendra2)Dcc) mice were obtained from Jackson Laboratory. Thpo−/− mice were produced inhouse by floxing exons 2 and 3 of the Thpo gene using CRISPR/Cas9 and subsequent germline excision by breeding with CMV-Cre mice. The CMV-Cre transgene was then bred out to generate Thpo−/− mice. Unless specified, 8 to 12-week-old mice were used in each experiment. Littermates of the same sex were randomly assigned to experimental groups. All animals were handled in strict accordance with good animal practice as defined by the Institution of Animal Care and Use Committee. All animal work was approved by the Institution of Animal Care and Use Committee and the Office of Safety, Health, and Environment at the National University of Singapore.

METHOD DETAILS

Flow cytometric analysis

Flow cytometric analysis was performed as described previously (Nakamura-Ishizu et al., 2012). Briefly, suspensions of bone marrow (BM) cells from the femurs, tibiae, spine and iliac crest of 8- to 12-week-old C57BL/6NTac mice were isolated and depleted of red blood cells by an ammonium chloride solution. The following antibodies were used for flow cytometric analysis. c-Kit (2B8)(Biolegend), Sca-1 (D7)(Biolegend), CD4 (RM4-5)(BD Bioscience), CD8 (53-6.72) (BD Bioscience), B220 (RA3-6B2) (BD Bioscience), TER-119 (TER-119)(BD Bioscience), Gr-1 (RB6-8C5) (BD Bioscience), CD34 (RAM34)(eBioscience), Mac-1 (M/70) (BD Bioscience), Flt-3 (A2F10.1)(eBioscience), CD41 (MWReg30)(BD Bioscience), CD45.2 (104)(Biolegend), CD45.1 (A20) (Biolegend), CD16/32 (2.4G2) (BD Bioscience), CD48 (HM48-1)(Biolegend), CD150 (TC15-12F12.2) (Biolegend), IL-7Rα (A7R34)(eBioscience), Endoglin (MJ7/18) (Biolegend), CD9 (KMC8)(BD Bioscience), Mpl (AMM2)(IBL), Ki67 (B56)(BD PharMingen), pSTAT3 (S727)(49)(BD Phosflow), GRIM19 (6E1BH7)(Abcam). For intracellular antigen staining, IntraPrep (Beckman Coulter) was used prior reaction with antibody. For mitochondrial staining, MitotrackerTM Green FM (ThermoScientific) and TMRE (Enzo) were used at concentrations specified by manufacturer. For intracellular ROS measurement CellROX (ThermoScientific) was used. For measuring ATP cell content, 50-1000 HSCs were sorted in 96-well plates containing 100μl of SFEM and assayed for luminescence using a CellTiter-Glo® 2.0 Assay (Promega) kit. We confirmed a linear relationship between HSC cell number and luminescence (R2 = 0.9995). Flow cytometric analysis and sorting was conducted on BD FACSAria II cell sorter.

BM Transplantation

BM MNCs (2 × 105 cells) from C57BL/6-Ly5.1 mice together with 20 LT-HSCs from mice C57BL/6N-Ly5.2 or UBC-GFP mice (Ly5.2) were transplanted into lethally-irradiated C57BL/6-Ly5.1 congenic mice. Secondary transplantations into lethally-irradiated C57BL/6-Ly5.1 congenic mice were performed using 2 × 10^6 BM MNCs from primary recipients. PB donor chimerism was analyzed monthly. Data was recorded for 10000 to 30000 MNCs for WBC chimerism (depending on the recovery of the PB) and 50000 events for RBC and platelet chimerism. Recipient mice were sacrificed for analysis 4 months after BMT.

In vitro HSC and Mk cultures

HSCs were sorted from WT mice were cultured in SFEM medium (Stem Cell technologies) supplemented with or without murine recombinant SCF (100ng/ml) and murine recombinant Thpo (100ng/ml) for 3 days and analyzed (Yoshihara et al., 2007). For inhibition experiments, FCCP (10uM) and KPT-330 (1uM) were supplemented to SFEM culture medium containing sorted HSCs 1-3 days. For Mk colony assay, 750 HSCs were plated for colony assay with MegaCult (Stem Cell Technologies) supplemented with rmThpo (50ng/ml), IL-3 (10ng/ml), IL-6 (20ng/ml) and IL-11 (50ng/ml) or MethoCult M3434 (Stem Cell Technologies). For myeloid colonies, 500uL of PB was pooled from 4 mice and plated for colony assay with MethoCult (M3234) (Stem cell Technologies). Colony counts for Mk colonies was assessed on day 10.

In vivo assays

Tissue samples from BMs were obtained as previously described (Petit et al., 2002). For *in vivo* stimulation of Thpo signaling, recombinant human Thpo (PEG-rHuMGDF) (Kabaya et al., 1996) (donated from Kyowa Hakko Kirin Co., Ltd.) was administered intravenously daily. Mice were treated with either 100 μg/kg (i.v.) PEG-rHuMGDF or human IgG Fc fragment (Jackson Immunoresearch). Romiplostim (Kyowa Kirin) or PBS for control was administered intravenously at a dose of 100 μg/kg (Léon et al., 2012). For G-CSF stimulation, 125μg/kgBW of Filgrastim (Kyowa Kirin) was subcutaneously injected to wild-type mice twice daily for 5 days.

Quantitative PCR assay

Total RNA was isolated using the RNeasy Mini Kit (QIAGEN) and was reverse transcribed with Superscript VILO (Invitrogen). Quantitative PCR assays were performed using an ABI 7500 Fast Real-Time PCR System, Taqman gene expression assays and Taqman Fast Universal PCR Master Mix (Applied Biosystems). Taqman gene expression assays (Applied Biosystems) used were *Ppargc1a*

(Mm01208835_m1), *Tfam* (Mm00447485_m1), *Nfe2l2* (Mm00477784_m1), *Nrf1* (Mm01135606_m1), *Sdhb* (Mm00458272_m1), *Sdhc* (Mm00481172_m1), *Atp5a* (Mm00431960_m1), *Cox5a* (Mm00432638_m1), *Cyc1* (Mm00470540_m1), *Ndufa13* (Mm00445751_m1) and *B2m* (Mm03003532_u1). Gene expression values were calculated using ΔΔCt method for the target genes by normalizing their expression to the Ct values for *B2m*.

Seahorse analysis

XF sensor cartridges were hydrated in XF Calibrant overnight at 37°C. HSPCs (LSK) were isolated from control and Romiplostim-treated mice into SFEM medium. Cells were cultured in SFEM at 37°C for 1 hour; cells from Romiplostim-treated mice were cultured in medium containing recombinant murine Thpo. Subsequently, HSPCs were washed and resuspended in Agilent Seahorse XF Base Medium. 330K cells were plated on onto one well of a Seahorse XFp culture plate coated with Cell-Tak reagent according to manufacturer's protocol. Cells were immobilized by centrifugation at 200xg for 3min at room temperature and were equilibrated in a humidified non-CO2 incubator for 20min. Cells were treated with 2.5uM of oligomycin, FCCP, rotenone and antimycin for analysis of mitochondrial respiration. Oxygen consumption rate (OCR) and extracellular acidification (ECAR) were measured with Seahorse XFe24 Analyzer (Seahorse Biosciences, North Billerica, MA).

RNA sequencing and gene set enrichment analysis

For single cell RNA sequencing, CD41+CD150+CD48-LSK cells from control and Thpo-treated mice were sorted into SFEM medium, centrifuged and re-suspended at a cell concentration of 600 cells per μl. Single cells were loaded on to C1 Single-Cell Auto Prep IFC (5-10μm diameter) for messenger RNA sequence using the Fluidigm C1 system. Cell viability of the loaded cells was assessed using LIVE/DEAD Viability/cytotoxicity Kit (Life Technologies) and imaging. Cells were lysed and whole transcriptome amplified cDNA was prepared using SMARTer Ultra Low RNA Kit for Fluidigm C1 system (Clonetech). Harvested cDNA samples were quantitated using Qubit Illumina libraries were constructed using Illumina Nextera XT DNA Sample Preparation Kit (Illumina) according to the manufacturer's protocol. Libraries were pooled, cleaned using Agencourt AMPure XP beads and sequenced on NextSeq500 system (Illumina) using Next-seq 500/550 High output Kit (75 cycles, single-end). 96 samples from a single group were placed on a single run to produce 4x108 reads.

Transmission Electron microscopy

Transmission Electron Microscopy was conducted as previously described with some modifications (Nakamura-Ishizu et al., 2008). In order to image small number of FACS sorted cells, cells were pre-stained with Evans blue for better detection of cell pellet (Kumar et al., 2014). Cell pellets were processed and embedded in Araldite resin and sectioned at 80nm using ultramicrotome Leica EM UC6. Sections were placed on a 200 mesh copper grid and imaged by JEOL JEM-1010.

Confocal microscopy and quantification of fluorescent images

Time lapse imaging for cell cycle analysis was conducted using cells isolated from Fucci transgenic mice. Isolated cells were placed on CytoCapture H20-10 chamber plates (Miltenyi Biotec) with SFEM medium supplemented with recombinant murine Thpo (100ng/ml) and SCF (100ng/ml) to reduce cell movement during imaging. Live cell imaging of was conducted using N-STORM/TIRF+ Live Cell Microscope. Cell analysis was conducted using NIS elements or ImageJ.

Super-resolution imaging

Sample preparation for STORM imaging was conducted as reported previously with some modifications (Dani et al., 2010). Briefly, sorted HSCs were stained for intra-cellular antigens using IntraPrep reagents (Beckman Coulter). Primary antibody for pSTAT3 (S727)(AlexaFluro647-conjugated)(BDPhosflow) and TOMM20 (Abcam) along with secondary antibody, AlexaFluro555 donkey anti-rabbit antibody (ThermoFisher Scientific) was used. Stained cells were seeded on a H250-100 cytocapture dish (Miltenyi). Immediately before imaging, cells were mounted with Permafluro medium (ThermoFisher Scientific) and covered with imaging medium freshly prepared. Imaging medium contained 7.7mg/ml Cysteamine (MEA), 0.7 mg/ml glucose oxidase, and 0.03 mg/ml catalase in 50mM Tris-HCl (pH8.0), 10mM NaCl and 10% glucose solution. Images were obtained using N-STORM/TIRF+ Live Cell microscope (Nikon) at Nikon Imaging Centre at Singapore Bioimaging Consortium. STORM imaging was performed for up to 3 hr after application of imaging medium. STORM images were analyzed using NIS elements NSTORM analysis software.

Mass cytometry

Heavy metal labeled antibodies were either purchased from Fluidigm or labeled using Maxpar antibody labeling kit (Figure S5A). Lineage marker negative (Lin-: CD4, CD8, B220, Gr1, Mac1, Ter119 negative) cells were isolated from control or Romiplostim-treated mice using MACS beads isolation. Isolated Lin- cells were stained for heavy metal labeled antibodies according to manufacturer's protocol. Briefly, cells were washed once with PBS and then stained with 1 μM cisplatin (Cell-ID Cisplatin, Fluidigm) for 5 min at room temperature to exclude dead cells. Cells were then fixed with MaxPar Fix I buffer (Fluidigm) and stained with anti-lineage-biotin antibodies in 50 μL of cell staining buffer (Fluidigm) for 30 min at room temperature (RT). Cells were washed with MaxPar cell stain buffer (Fluidgm) and stained with heavy-metal labeled surface marker antibodies in 50 μL of cell staining buffer for 30 min at RT. Cells were washed twice and permeabilized with 500 μL of methanol on ice for 15 min. Cells were then stained with heavy-metal labeled

cytoplasmic and nuclear antibodies in 50 μL of cell staining buffer for 30 min at RT, washed and resuspended in 1ml of intercalation solution containing Cell-ID Intercalator-Ir (Fluidigm) for 1hr at RT, washed and resuspended in Maxpar water for data acquisition on Helios (Fludigm). tSNE analysis was conducted using Cytobank.

QUANTIFICATION AND STATISTICAL ANALYSIS

Single cell RNA sequencing analysis

Single-end reads were aligned to the *Mus musculus* genome (mm10) using Bowtie 2 (Langmead and Salzberg, 2012) and differentially expressed genes (DEGs) between Thpo treatment groups were determined using Cufflinks v2.2.1 (Trapnell et al., 2013). In order to reduce the number of spurious results due to low overall expression within either population, a minimum expression threshold was imposed to exclude DEGs that were absent in > 50% of cells. Cells with less than 375 expressed genes were considered of low quality and removed. Dimensionality reduction and visualization were performed using the Rtsne package (version 0.13) with standard parameters in the software package R (version 3.3.2).

Gene-set and gene-ontology enrichment analyses

Enrichment of cell type specific gene sets among DEGs was determined using Fishers exact test. Mk gene sets (MkP and PreMEGE) were retrieved from a previously published dataset by Sanjuan-Pla et al. (Sanjuan-Pla et al., 2013). Furthermore, enrichment of pathway specific gene sets was performed using PANTHER (release 20160715) (Mi et al., 2017) using Reactome version 58 and a significance level of $\alpha < 0.05$ with Bonferroni correction for multiple testing. More general over-representation of gene-ontology terms was assessed using GSEA v2.0.13 software (Subramanian et al., 2005). Here, the number of permutations was set at 1000 and gene sets with a nominal p value < 0.05, and false discovery rate q value (FDR-q) < 0.25 were considered statistically significant.

Mass Cytometry data analysis

Raw CyTOF data was processed in R (version 3.4.2) using the flowCore, flowViz and flowUtils packages. Data was transformed with Data was transformed with

$$f(x) = \frac{\operatorname{asinh}\left(t + \frac{x}{\gamma}\right)}{\log(10)} + c$$

where t = 0.43429448190325176, γ = 5.8760059682190064 and c = 0 and gates defined in Cytobank were applied to data. To determine the effect of Romiplostim treatment on individual features, a Random Forest consisting of 500 trees was grown using the R-package randomForest. To account for differences in cell numbers across replicates, stratified re-sampling of 1000 measurements with replacement from four untreated and four treated replicates was employed to obtain a training dataset consisting of 8000 single-cell protein expression profiles and corresponding treatment labels. Classification certainty was determined as the area under the curve (AUC) of the receiver operator characteristic (ROC) curve using the out-of-bag samples and importance of features was determined using the Gini index.

Statistical analysis

Statistical details of experiments can be found in Figure legends. All results are expressed as the mean ± SD unless otherwise specified. Statistical significance was determined by Tukey's multiple comparison test. The two-tailed Student's t test was used for two-group comparisons. All experiments were repeated in at least two independent experiments.

DATA AND SOFTWARE AVAILABILITY

The accession number for the raw single cell RNA-sequencing data reported in this paper is GEO: GSE121001.